### Unimolecular reaction rate theory for transition states of partial looseness. II. Implementation and analysis with applications to NO2 and C2H6 dissociations

David M. Wardlawa) and R. A. Marcus

Arthur Amos Noyes Laboratory of Chemical Physics, California Institute of Technology, b) Pasadena, California 91125

(Received 22 April 1985; accepted 6 June 1985)

Implementation of RRKM theory for unimolecular dissociations having transition states of any degree of looseness is described for reactions involving dissociation into two fragments. The fragments may be atomic, diatomic, or polyatomic species. Action-angle and internal coordinates for the transitional modes of the reaction, transformations to Cartesian coordinates, and other calculational aspects are described. Results for the  $NO_2 \rightarrow NO + O$  reaction are presented, including the dependence of the microcanonical rate constant on the bond fission and bending potentials for model potential energy surfaces. Illustrative calculations for the C<sub>2</sub>H<sub>6</sub>→2CH<sub>3</sub> reaction are also given.

#### I. INTRODUCTION

Frequently the transition state of a reaction is defined in terms of the position of some maximum (saddle point) in the potential energy surface along the reaction coordinate. However, in reactions such as certain unimolecular dissociations to free radicals (and, hence, recombination of free radicals) and some ion-molecule reactions, a local potential energy barrier maximum may be absent. A method was presented in part I1 for implementing RRKM theory for such reactions, and it was illustrated for the dissociation  $H_2O_2 \rightarrow 2OH$ . In the present paper the coordinates, the transformations between coordinate systems, and the evaluation of the phase space integral arising in this formulation are described in some detail. Illustrative results are given for the reactions  $NO_2 \rightarrow NO + O$  and  $C_2H_6 \rightarrow 2CH_3$ .

The rate constant  $k_{EJ}$  of a unimolecular reaction is given in RRKM theory<sup>2</sup> as a function of the energy E of the molecule (in the center-of-mass frame) and of the total angular momentum J.

$$k_{EJ} = \frac{N_{EJ}}{h\rho_{EJ}},\tag{1}$$

where  $N_{EJ}$  is the number of quantum states of the transition state having at the given J an energy less than or equal to E in all degrees of freedom but the reaction coordinate, and  $ho_{EJ}$  is the density of states of the dissociating or isomerizing molecule. Tunneling corrections along the reaction coordinate and any reaction path degeneracy can be introduced into  $N_{EJ}$  if needed.<sup>3</sup> A unimolecular rate constant at any pressure is obtained from Eq. (1) in the standard way by suitably weighting the contributions from different E's and J's [Eq. (4) of Ref. 4]. The main idea for calculating  $N_{EI}$ , described in part I, is that the degrees of freedom are subdivided into "transitional" ones and the remaining coordinates, in a center-of-mass system of coordinates. The transitional degrees of freedom involve (a) the bending motions of the two parts of the dissociating molecule, which become free rotations in the

products, (b) the relative orbital motion of the separating fragments, and (c) the other coordinates, if any, which change considerably their form of motion during the progress of the molecule along the reaction coordinate. These various motions are typically strongly coupled to each other and are constrained by energy and total angular momentum conservation. Such coupling and constraints make a purely quantum mechanical calculation of the energy levels of the system at each value of the reaction coordinate formidable. The contribution  $\Omega_I(\epsilon)$  of such coordinates to  $N_{EI}$  as a function of their energy E can be calculated from an evaluation of the corresponding classical phase space integral, introducing quantum corrections<sup>3</sup> if necessary.

With this subdivision of the coordinates into two groups  $N_{EI}$  can be written as<sup>1</sup>

$$N_{EJ} = \int_{0}^{E'} N_{\nu}(E' - \epsilon) \Omega_{J}(\epsilon) d\epsilon, \qquad (2)$$

where  $\Omega_{J}(\epsilon)d\epsilon$  is the number of quantum states of the transitional modes for the given J when their total energy lies in the interval  $(\epsilon, \epsilon + d\epsilon)$ ,  $N_{\nu}(E' - \epsilon)$  is the number of quantum states in the remaining coordinates when their energy is less than or equal to  $E' - \epsilon$ , E' being the available energy, i.e., E minus the value of the potential energy minimum at the given value of the reaction coordinate and minus the zero point energy of the modes included in  $N_{\nu}$ . The two types of coordinates are taken to be uncoupled from each other in Eq. (2), apart from an indirect coupling via the dependence of the molecular constants on the reaction coordinate. The value of  $N_{\nu}$  in Eq. (2) is obtained by the usual quantum count, while  $\Omega_{J}(\epsilon)$  and  $N_{EJ}$  are evaluated by Monte Carlo methods. The minimum value of  $N_{EJ}$  along the reaction coordinate is then used to define the transition state<sup>5</sup> and, thereby, the value of  $N_{EJ}$  to be introduced for the numerator in Eq. (1). The quantity  $\Omega_I(\epsilon)$  itself can be evaluated either by using action-angle variables, as in part I, or by using constrained internal coordinates. In the present paper the former are used.

The application of RRKM theory described in part I and in this paper foregoes the considerable simplicity afforded by largely analytical expressions<sup>4,6</sup> for  $N_{EJ}$ , in favor of a

a) Present address: Department of Chemistry, Queens University, Kingston, Ontario, K7L 3N6 Canada.

b) Contribution No. 7186.

more accurate physical treatment of the transition state for this more general case. The principal ingredients for calculating  $N_{EJ}$ , apart from the quantum count of  $N_V$  involve some tedious though relatively straightforward and readily programmed transformations and a Monte Carlo calculation. The results serve to identify the more important parts of the potential energy surface for the reactions concerned. They can be used as a basis for selecting suitable points for the calculation of improved potential energy surfaces for studying the rates of these reactions.

The present article is subdivided as follows: In Sec. II and the Appendices, the action-angle coordinates are given for the transitional modes, together with the transformations to the internal or relative coordinates. The subsequent evaluation of  $N_{EJ}$  is discussed in Sec. III and details of the Monte Carlo sampling, integration limits in the calculation of  $\Omega_I(\epsilon)$ , and the counts used for  $N_V$  are given in an Appendix. The theory is applied to the NO<sub>2</sub>→NO + O reaction in Sec. IV for a model potential surface (Appendix A), and compared with the theoretical results from the statistical adiabatic-channel model (SACM). The effect on  $N_{EJ}$  (and hence on  $k_{EI}$ ) of varying the bending and bond-fission potential energy functions is also investigated for this reaction. The potential energy surface used and the transformation from actionangle to internal coordinates for the H<sub>2</sub>O<sub>2</sub>->2 OH reaction studied in part I are given in Appendices. Some illustrative results for the  $k_{EJ}$  of the  $C_2H_6\rightarrow 2CH_3$  reaction are given in Sec. V. A full account of the present treatment applied to this reaction, and comparisons with experimental data, are given later. The C<sub>2</sub>H<sub>6</sub> coordinate transformations and the methods given here are applicable to more general systems with larger polyatomic fragments. The  $N_{EJ}$  calculations of Secs. IV and V are discussed in Sec. VI and conclusions follow in Sec. VII.

#### II. ACTION-ANGLE VARIABLES, INTERNAL COORDINATES, AND DENSITY OF STATES

To calculate  $\Omega_J(\epsilon)$  in Eq. (2) two sets of body-fixed coordinate axes are first defined, each fixed in a separating fragment. 1,8,9 The origin of each system is located at the center of mass of that fragment, and when either fragment has some symmetry its coordinate axes are chosen to coincide with its symmetry axes. A third set of body-fixed coordinates is also defined, fixed in the molecule as a whole. For the coordinates of the transitional modes the action-angle coordinates described previously<sup>1,8-10</sup> are then introduced. In the following and in Appendices, the action-angle variables are defined for three different classes of reacting systems of increasing complexity, represented by the reactions  $NO_2 \rightarrow NO + O$ ,  $H_2O_2 \rightarrow 2OH$ , and  $C_2H_6 \rightarrow 2CH_3$ . The transformation of the action-angle variables to internal displacement plus separation distance coordinates, in which the potential energy function is usually expressed, is also described. These three reactions have two, four, and six transitional modes, respectively, and are prototypes for dissociation into an atom and a linear fragment, into two linear fragments, and into two nonlinear fragments.

Angular momentum action-angle variables for a nonlinear system such as  $ABC \rightarrow AB + C$  (e.g.,  $NO_2 \rightarrow NO + O$ )

can be chosen to be  $j, j_z, l, l_z$  (written here and throughout in units of  $\hbar = 1$ )<sup>11</sup> and their conjugate angles  $\alpha_j$ ,  $\beta_j$ ,  $\alpha_l$ ,  $\beta_l$ . (Two distances and their conjugate momenta complete the set of variables in the center-of-mass system of coordinates.) The angles range over a  $2\pi$  interval. The variables j and  $j_z$  describe the rotational angular momentum and the space-fixed z component of the diatomic AB, respectively; l and  $l_z$  denote the orbital angular momentum of the fragments and its z component. The conjugate angles are angle variables in the planes perpendicular to the corresponding angular momentum vectors. It is convenient to use instead the variables  $(J,\alpha,J_z,\beta)$  obtained in a canonical transformation  $^{9,10}$ 

$$(j_z,\beta_i,l_z,\beta_l) \rightarrow (J,\alpha,J_z,\beta),$$
 (3)

where  $J(=|\mathbf{j}+\mathbf{1}|)$  is the action for the total angular momentum,  $J_z$  is its space-fixed component, and  $\alpha$ ,  $\beta$  are their respective conjugate angles. For a system so described and for a given value of J the semiclassical value  $\Omega_J$  of quantum states of the transitional modes is

$$\Omega_{J}(\epsilon) = (2\pi)^{-4}\sigma^{-1} \int \cdots \int \times dJ_{z} \, dj \, dl \, d\alpha \, d\beta \, d\alpha_{j} \, d\alpha_{l} \, \Delta \, (J,j,l) \delta(\epsilon - H_{\rm cl})$$
(4)

(in units of  $\tilde{n}=1$ ). Here,  $H_{\rm cl}$  is the classical Hamiltonian for the transitional modes and is given below.  $\Delta (J,j,l)$  is unity when the triangle inequality |j-l| < J < j+l is fulfilled and zero otherwise. The integration limits for the angle variables are  $(0, 2\pi)$ .  $\sigma$  is a symmetry number which corrects for the overcounting of any indistinguishable configurations in these  $(0, 2\pi)$  angle intervals. The angular momentum actions j and l are restricted by energy conservation and the limits on the  $J_z$  integral are (-J,J).

The Hamiltonian  $H_{cl}$  for the transitional modes is written as

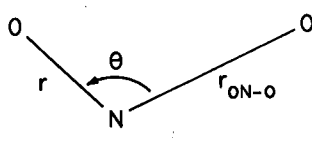
$$H_{\rm cl} = \frac{f^2}{2\mu_{\rm AB}r^2} + \frac{l^2}{2\mu R^2} + V_t(r_{\rm AB-C}, \theta), \tag{5}$$

where  $\mu_{AB}$  is the reduced mass of AB,  $\mu$  is the reduced mass for the relative motion of AB and C, and R is the distance between C and the center of mass of AB. The potential  $V_t$  for the transitional modes is modeled in the present study so as to be a function of the internal coordinates  $r_{AB-C}$  and  $\theta$  depicted in Fig. 1(a). The other coordinate r in Fig. 1(a) corresponds to the AB bond length and that vibration contributes instead to the quantum state count in  $N_V(E'-\varepsilon)$ . The reaction coordinate R, the angular momenta j and l, and the angle  $\gamma$  between R and r are depicted in Fig. 1(b). The functional form and numerical parameters used for  $V_t$  are given in Appendix A and for more complex systems in Appendices B and C.

To evaluate  $V_t$  in Eq. (5), the internal coordinates,  $r_{AB-C}$  and  $\theta$  are first expressed in terms of the Jacobi coordinates  $(R, r, \gamma)$  as in Appendix A. For any R, r is then replaced by its R-dependent equilibrium value  $r_e$  (Appendix A), and  $\gamma$  is expressed in terms of J and the action-angle variables appearing in Eq. (4):

$$\cos \gamma = \cos \alpha_i \cos \alpha_l + \sin \alpha_j \sin \alpha_l \cos \theta_{ij}, \tag{6}$$





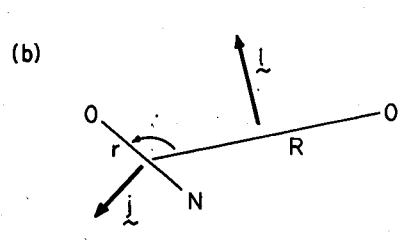


FIG. 1. (a) The N-O length r, the bond dissociation coordinate  $r_{\text{ON-O}}$ , and the bending angle  $\theta$  for the NO<sub>2</sub> $\rightarrow$ NO + O system. (b) Angular momenta for the NO fragment rotation and for the orbital motion of ON and O; R is the distance between the centers of mass, and  $\gamma$  is the angle between  $\mathbf{r}$  and  $\mathbf{R}$ .

where  $\theta_{ij}$  is the angle between l and j and is given as a function of l, j, and J in Table II. The angles  $\gamma$ ,  $\alpha_j$ , and  $\alpha_l$  are depicted in Fig. 2 and, together with other angles, are specified in Tables I and III. The form of Eq. (6) applies to the various other systems of angles used in this paper and such results systematically follow from the identity<sup>12</sup>

$$(\mathbf{a} \times \mathbf{b}) \cdot (\mathbf{c} \times \mathbf{d}) = (\mathbf{a} \cdot \mathbf{c})(\mathbf{b} \cdot \mathbf{d}) - (\mathbf{a} \cdot \mathbf{d})(\mathbf{b} \cdot \mathbf{c}), \tag{7}$$

with a, b, c, and d identified in Table III.

In the above way  $V_t$ , and hence  $H_{cl}$ , are specified by the variables  $(R,r,J,j,l,\alpha_j,\alpha_l)$ . The latter determine only the relative positions of the atoms. Hence,  $V_t$  and  $H_{cl}$  are independent of the variables  $(J_z,\alpha,\beta)$ , which determine the overall orientation of the body-fixed frame, <sup>10</sup> permitting the integral in Eq. (4) to be simplified to

$$\Omega_{J}(\epsilon) = (2J+1)(2\pi)^{-2}\sigma^{-1}\int \cdots \int \times dj \ dl \ d\alpha_{i} \ d\alpha_{l} \Delta (J,j,l)\delta(\epsilon - H_{cl}), \tag{8}$$

which, combined with Eq. (2), yields

TABLE I. Definition of Euler angles conjugate to various angular momenta.<sup>a</sup>

System	Angular momentum	Conjugate angle	Reference axis x	Rotated axis y
NO <sub>2</sub>	1	$\alpha_l$	lxj	R,
-	$oldsymbol{j}$	$oldsymbol{lpha_j}$	l×j	r
$H_2O_2$	1	$\alpha_l$	l×k	R
2 2	$\boldsymbol{k}$	$\alpha_k$	l×k	$\mathbf{j}_1 \times \mathbf{j}_2 = \mathbf{j}_1 \times$
	$j_i$	$\alpha_i$	$\mathbf{j}_1 \times \mathbf{j}_2$	$\mathbf{r}_i$ . "
C <sub>2</sub> H <sub>6</sub>	1	$\alpha_{i}$	l×k <sup>b</sup>	R
2 0	$\boldsymbol{k}$	$\alpha_k$	l×k⁵	$\mathbf{j}_1 \times \mathbf{j}_2 = \mathbf{j}_1 \times$
	$j_i$	$\alpha_i$	l×j,°	$\kappa_i  imes \mathbf{j}_i$
	K <sub>i</sub>	$\gamma_i$	$\kappa_i \times j_i^d$	<b>e</b> <sub>x''</sub>

All angles range from 0 to  $2\pi$  and are obtained by counter-clockwise rotation about  $x \times y$  from x to y (Ref. 12). The subscript i refers to fragment 1 or

$$N_{EJ} = (2J+1)(2\pi)^{-2}\sigma^{-1} \int \cdots \int \times dj \, dl \, d\alpha_i \, d\alpha_l \, N_V(E'-H_{cl}) \Delta \, (Jj,l), \tag{9}$$

the desired relation. In Eq. (9)  $N_{\nu}(E'-H_{\rm cl})$  is zero when  $E' < H_{\rm cl}$ . The evaluation of the integral in Eq. (9) is described in Sec. III.

The foregoing equations and concepts are extended to more complex reacting systems in Appendices D and E. Various relevant angles are depicted in Figs. 3 and 4. The case of J=0 is typically unimportant, since it is only one point on a distribution of many J's. Nevertheless, it is given for completeness in Appendix G for the various systems.

#### III. EVALUATION OF $N_{EJ}$

In evaluating the integral for  $N_{EJ}$  appearing in Eq. (9) [and in Eqs. (D9) and (E8)] by analytical or quadrature methods one encounters relatively high dimensionality (4 to 12), interdependent integration limits, and an integrand in which

TABLE II. Definitions of angles contained between various angular momenta.<sup>a</sup>

System	Angular momentum pair	Angle $\chi$	$\cos \chi$
NO <sub>2</sub>	(l,j)	$\theta_{lj}$	$(J^2-l^2-f^2)/2lj$
$H_2O_2, C_2H_6$	(l, k)	$ heta_{lk}$	$(J^2 - l^2 - k^2)/2lk$
2,2 2 3	$(j_1,j_2)$	$\theta_{12}$	$(k^2-j_1^2-j_2^2)/2j_1j_2$
	$(k, j_1)$	$\theta_{k1}$	$(j_1^2 + k^2 - j_2^2)/2j_1k$
	$(k, j_2)$	$\theta_{k2}$	$(j_2 + k^2 - j_1^2)/2j_2k$
\$ 5	$(l,j_1)$	$\theta_{l1}$	$\cos \theta_{lk} \cos \theta_{k1} + \sin \theta_{lk} \sin \theta_{k1} \cos \alpha_k^b$
	$(l,j_2)$	$\theta_{l2}$	$\cos \theta_{lk} \cos \theta_{k2} - \sin \theta_{lk} \sin \theta_{k2} \cos \alpha_k^b$

In all cases  $0 < \theta < \pi$  and  $\sin \theta$  is obtained from  $\cos \theta$  as the positive root.

<sup>&</sup>lt;sup>b</sup> Corresponds to axis x in Fig. 4(a).

<sup>°</sup> Corresponds to the line of nodes  $N'_i$  in Fig. 4(a) for i = 1.

<sup>&</sup>lt;sup>d</sup> Corresponds to the line of nodes  $N_1$  in Fig. 4(a) for i = 1.

<sup>&</sup>lt;sup>b</sup> These expressions are obtained from Eq. (7) with  $\mathbf{a} = \mathbf{l}$ ,  $\mathbf{b} = \mathbf{d} = \mathbf{k}$ , and  $\mathbf{c} = \mathbf{j}_i$ ; the sign difference arises because  $\alpha_k$  is the angle between  $\mathbf{l} \times \mathbf{k}$  and  $\mathbf{j}_1 \times \mathbf{k} = \mathbf{j}_1 \times \mathbf{j}_2$  (see Table I), whereas  $\pi + \alpha_k$  is the angle between  $\mathbf{l} \times \mathbf{k}$  and  $\mathbf{j}_2 \times \mathbf{k} = -\mathbf{j}_1 \times \mathbf{j}_2$ .

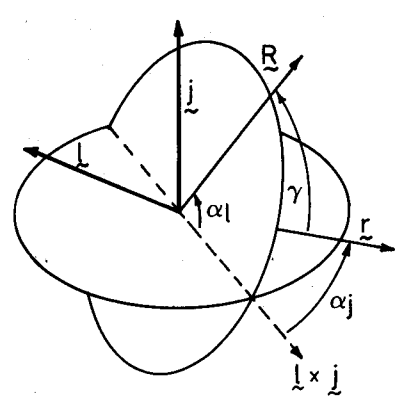


FIG. 2. An Euler diagram depicting the various angles involved in describing the transitional degrees of freedom for an atom plus diatom system. The planes in which  $\mathbf{R}$  and  $\mathbf{r}$  lie are perpendicular to  $\mathbf{l}$  and  $\mathbf{j}$ , respectively. The two planes intersect along the line of nodes  $\mathbf{l} \times \mathbf{j}$ .  $\alpha_l$  and  $\alpha_j$  are angles conjugate to l and j, respectively, and  $\gamma$  is the angle between  $\mathbf{R}$  and  $\mathbf{r}$ . For pictorial clarity the angle  $\theta_{ij}$  between  $\mathbf{l}$  and  $\mathbf{j}$  is not shown. All Euler angles are defined by a right-hand rule, i.e., they describe a counterclockwise rotation in the plane perpendicular to the axis of rotation.

all variables of integration are coupled via  $V_t$ , which itself is a complicated function of the new variables. Such integrals are well suited to evaluation by Monte Carlo methods. <sup>13</sup> One may write

$$N_{EJ} = N_{EJ}^{\text{MC}} \pm \sigma^{\text{MC}},\tag{10}$$

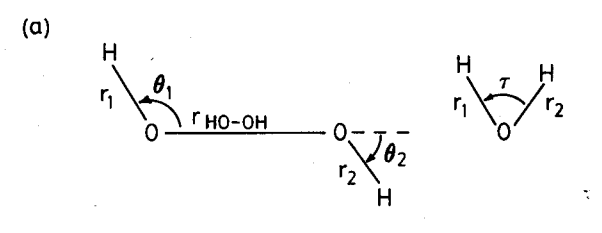
where  $N_{EJ}^{\rm MC}$  and  $(\sigma^{\rm MC})^2$  are Monte Carlo estimates of  $N_{EJ}$  and of the variance  $\sigma^2$  of  $N_{EJ}^{\rm MC}$ , respectively.

In this paper, which is aimed mainly at examining the salient features of the present method, we have found it expedient to use the crude Monte Carlo method for evaluating  $N_{EJ}^{\rm MC}$  and  $\sigma^{\rm MC}$ , namely to use a uniform sampling of all variables, combined with a weighting method <sup>13</sup> for coping with the awkward interdependent integration limits. The details of the calculation, including the counts for  $N_{\nu}$ , are given in Appendix F. Also described are some elementary procedures which reduced the variance  $(\sigma^{\rm MC})^2$  for the transitional modes. Other more sophisticated Monte Carlo techniques for evaluating  $N_{EJ}$  can, of course, also be used.

Monte Carlo calculations of phase space volumes have been used in completely classical calculations of numbers of states, densities of states, and unimolecular rate theory. Both rotating <sup>14</sup> and nonrotating <sup>15–18</sup> systems have been so studied, although for the rotating systems <sup>14</sup> the ensembles were

TABLE III. Identification of vectors used to define cosines of various angles via Eq. (7).

System	Angle	8	b	c	d
NO <sub>2</sub>	γ	l×j	r .	l×j	R
$H_2O_2$	λ	$\mathbf{r}_1$	R	r <sub>2</sub>	R
·	$\varphi$	$\mathbf{j}_1 \times \mathbf{j}_2$	$\mathbf{r}_1$	$\mathbf{j}_1 \times \mathbf{j}_2$	$\mathbf{r}_2$
	$\gamma_i$	$\mathbf{j}_1 \times \mathbf{j}_2$	$\mathbf{r}_{i}$	l×k	R
	$\theta_R$	l×k	R	l×k	$\mathbf{j}_1 \times \mathbf{j}_2$
	$\theta_{r_i}$	$\mathbf{j}_1 \times \mathbf{j}_2$	$\mathbf{r}_i$	l×k	$\mathbf{j}_1 \times \mathbf{j}_2$
$C_2H_6$	$\beta_i$	1	k	1	$\mathbf{j}_i$



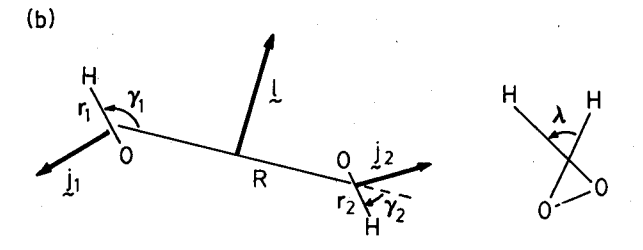


FIG. 3. (a) The OH bond lengths  $r_1$  and  $r_2$ , bond dissociation coordinate  $r_{\text{OH-OH}}$ , bending angles  $\theta_1$  and  $\theta_2$ , and torsional angle  $\tau$  for the  $H_2O_2\rightarrow 2OH$  system. (b) Angular momenta for fragment rotations and for the relative motion of  $HO\cdots OH$ , the distance R between the centers of mass, the angles  $\gamma_1$  between R and  $r_i$  (i=1,2), and the angle  $\lambda$  between the plane defined by  $r_1$  and R and that defined by  $r_2$  and R.

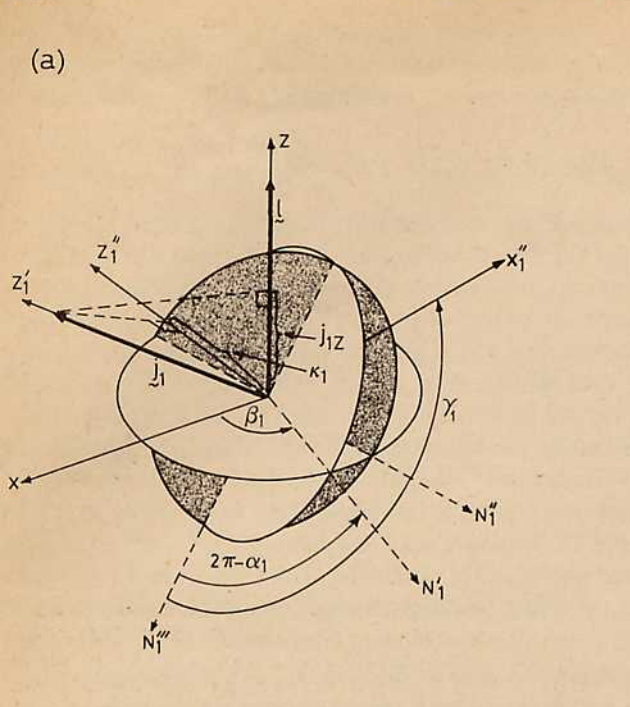
not J fixed. In a study<sup>17</sup> of the vibrational predissociation of the Ar–BCl<sub>3</sub> van der Waals' molecule a generalization<sup>15(b)</sup> of Slater theory was used to obtain  $k_E$ 's via Metropolis sampling. A similar approach was used<sup>18</sup> in a study of the unimolecular dissociation of methane. The results for CH<sub>4</sub> $\rightarrow$ CH<sub>3</sub> + H were converged, though an uncertainty of  $\sim$  100% was reported for the Monte Carlo estimates of  $k_E$  for CH<sub>4</sub> $\rightarrow$ CH<sub>2</sub> + H<sub>2</sub>, due to the excessive computational times needed for convergence.

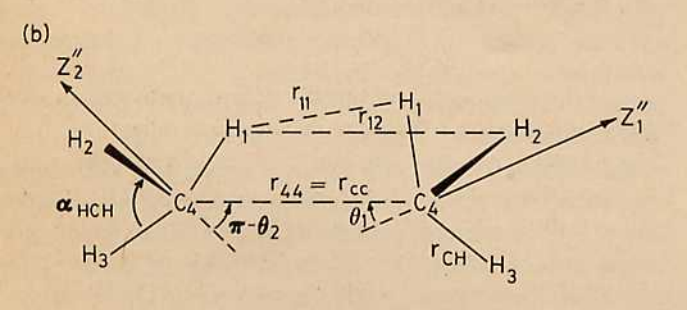
## IV. RESULTS FOR THE REACTION NO<sub>2</sub>→NO + O A Calculations for N , we F and / and comparison w

## A. Calculations for $N_{EJ}$ vs E and J and comparison with SACM

Results for  $N_{EJ}$ , the quantity useful for assessing the accuracy and computational facility of the present method, are described in this section. Using a model potential energy surface described in Appendix A, results for  $N_{EJ}$  [with  $\sigma=1$  in Eq. (9)] were obtained for several J's and are plotted in Fig. 5 vs  $E'_{\infty}$ , the energy of the separated products in excess of their zero point and potential energy.

To obtain  $N_{EJ}$  at the "bottleneck" value of R,  $R^{\dagger}$ , i.e., at the location of the minimum in the reactive flux, the integral in Eq. (9) was evaluated as a function of R at fixed intervals (0.1 Å for this reaction) using the Monte Carlo method described in Sec. III and Appendix F. The accuracy of the present Monte Carlo estimates of  $N_{EJ}$  as measured by  $\sigma^{\rm MC}/N_{EJ}^{\rm MC}$ , was at worst  $\sim 1.5\%$  for all values of R. The relative accuracy was found to depend only on the number of integration points and was essentially independent of  $E'_{\infty}$  and of J. The fraction of rejected Monte Carlo integration points increases as R decreases as a result of more severe configurational restrictions imposed by the transitional mode potential at smaller R. In order to maintain the relative accuracy at  $\lesssim 1.5\%$  for all R values it was therefore neces-





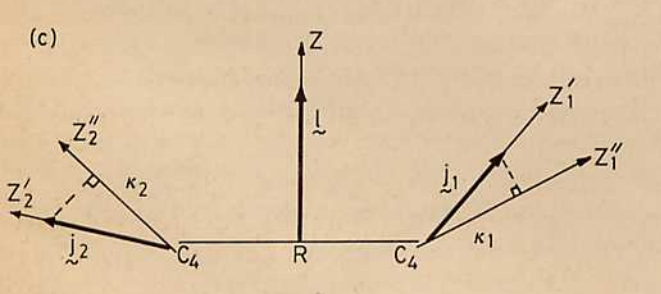


FIG. 4. (a) Euler diagram depicting the relationship between the (x, y, z),  $(x'_1, y'_1, z'_1)$ , and  $(x''_1, y''_1, z''_1)$  Cartesian coordinate systems for the nonlinear polyatomic fragment 1. I lies along the z axis,  $j_1$  along the  $z'_1$  axis, and  $\kappa_1$  is the projection of j, on the z" axis. Pairs of the three xy planes intersect along the lines of nodes  $N'_1$ ,  $N''_1$ , and  $N'''_1$ , whose orientations are determined by the vectors  $\mathbf{l} \times \mathbf{j}_1$ ,  $\mathbf{l} \times \kappa_1$ , and  $\kappa_1 \times \mathbf{j}_1$ , respectively;  $N_1'''$  also serves as the  $x_1'$ axis. The angles  $(\alpha_1, \theta_{I1}, \beta_I)$  are the Euler angles specifying the orientation of the primed system relative to the unprimed system and the angles ( $\gamma_1$ ,  $\theta_{K1}$ , 0) are those specifying the orientation of the primed system relative to the doubly primed system. For pictorial clarity, the angle  $\theta_{I1}$  between the z axis and the  $z_1'$  axis and the angle  $\theta_{\kappa 1}$  between the  $z_1'$  axis and the  $z_1''$  axis are not shown. (b) The CH bond length  $r_{CH}$ , the angle between adjacent CH bonds  $\alpha_{HCH}$ , the bond dissociation coordinate  $r_{CC} = r_{44}$ , several interfragment atomic separation coordinates  $r_{ij}$ , and the angles  $\theta_i$  between  $r_{\rm CC}$  and the symmetry axis  $z_i''$  of fragment i (i = 1, 2) for the  $C_2H_6 \rightarrow 2$  CH<sub>3</sub> system. The carbon atom of fragment 2 is taken as the origin of rcc. (c) Angular momenta for fragment rotations and for the orbital motion of H<sub>3</sub>C···CH<sub>3</sub>, the distance R between the centers of mass, and the projection  $\kappa_i$  of  $j_i$  on the z" axis.

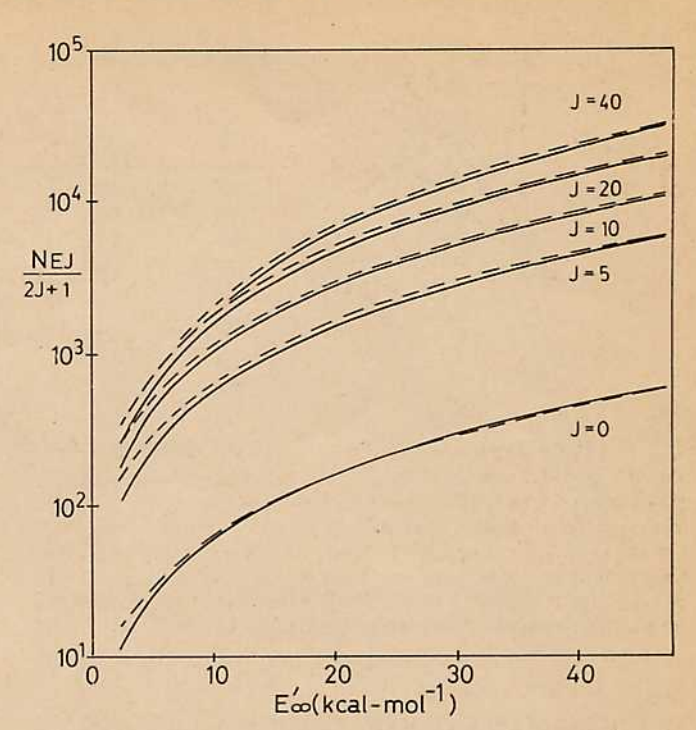


FIG. 5. Semilog plot of  $N_{EJ}/(2J+1)$  vs  $E_{\infty}'$  in units of kcal mol<sup>-1</sup> for various values of the total angular momentum J for NO<sub>2</sub> $\rightarrow$ NO + O.  $E_{\infty}'$  is the energy available to the system at  $R=\infty$ . The solid curves depict the present results and the dashed curves are obtained from a statistical adiabatic-channel model (SACM) calculation. The statistical uncertainty in the  $N_{EJ}$  at  $R^{\dagger}$  values resulting from the Monte Carlo calculation is too small to be resolved on the scale of the figure and has been omitted.

sary to increase the absolute number of points smoothly from 3000 in the region of zero potential  $(R = \infty)$  to 35 000 at R = 1.9 Å, the smallest separation considered.

The present method can be used with any potential energy surface, *ab initio* or semiempirical. However, for purposes of this paper the potential energy function (Appendix A) used was designed so as to facilitate a comparison with statistical adiabatic channel model (SACM)<sup>19</sup> calculations. In the latter, outlined in Appendix H, vibrationally adiabatic channel curves are constructed by assuming that a universal interpolating function<sup>19</sup> smoothly connects reactant and product eigenvalues. The surface specified in Appendix A leads to molecular parameters which would approximately yield this interpolation formula. The SACM calculated results are also given in Fig. 5 as a function of energy for various *J*'s.

To determine the extent of looseness of the transition state, the value of  $N_{EJ}(R^{\dagger})$  was compared with the value at  $R = \infty$ ,  $N_{EJ}(\infty)$ , for various E's and J's. For J's of 0, 20, and 40, the ratio  $N_{EJ}(R^{\dagger})/N_{EJ}(\infty)$  varied over the intervals (0.53 to 0.89), (0.48 to 0.86), and (0.36 to 0.81), respectively, when  $E'_{\infty}$  was varied from 2.29 to 47.29 kcal mol<sup>-1</sup>.

#### B. Dependence of $N_{E,l}$ on the potential energy function

In the absence of accurate theoretical calculations for the interfragment potentials in the region of separation distances of interest—frequently two to five times the equilibrium bond length for simple bond-fission reactions—it is common to use a Morse function to model the bond-fission part

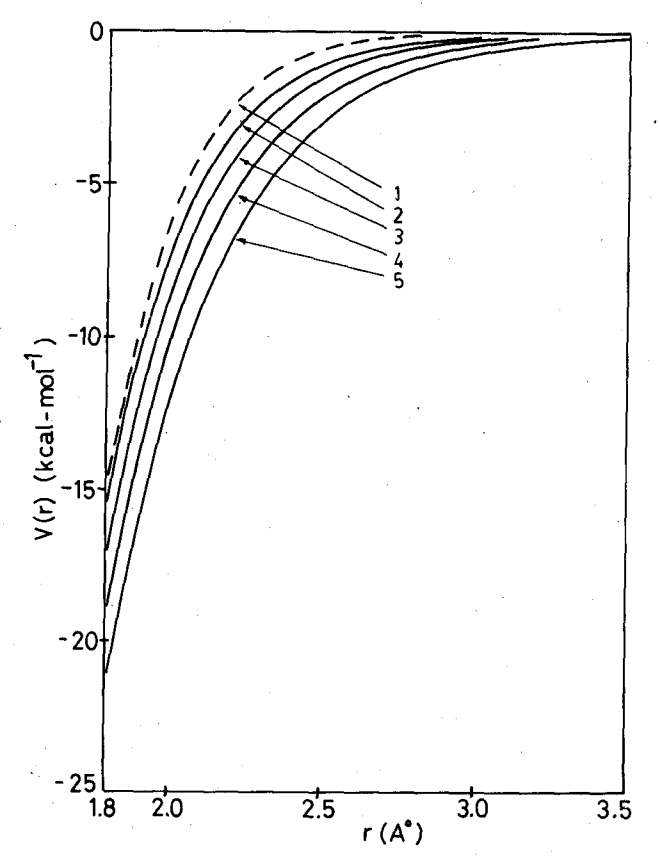


FIG. 6. The various bond dissociation potential energy curves used in the model potential energy surface for the  $NO_2 \rightarrow NO + O$  system are depicted. Only the range 1.8-3.5 Å is shown and V=0 corresponds to separated fragments. Curve 1 is a Varshni potential, curve 4 a Morse function, and curves 2, 3, and 5 are Morse functions modified by altering  $\beta$  as described in the text.

of the potential energy function  $V_t$  in Eq. (5). <sup>19,20</sup> However, for many diatomic molecules the Morse function is often inaccurate at larger separation distances, usually being lower than the experimentally based RKR potential curve and rising less steeply as the bond length is increased. <sup>19,21</sup> Accordingly, the sensitivity of  $N_{EJ}$  to modifications of the bond-fission potential  $V_{\rm bf}$  was examined next.

One approach to obtaining improved potential curves is

to let the Morse parameter  $\beta$  depend on the bond length or reaction coordinate.<sup>22</sup> For simplicity,  $\beta(R)$  now has the form

$$\beta(R) = \beta_{\infty} + (\beta_{M} - \beta_{\infty})g(R), \tag{11}$$

where g(R) is an interpolation function,  $\beta_{M}$  is the Morse value for the ON-O bond (given later in Table A1), and  $\beta_m$  is chosen to have several different values. The function g(R)was chosen to be that given in Eq. (A2). The potential energy curves labeled 2, 3, 4, and 5 in Fig. 6 correspond to choices of  $\beta_{\infty}$  such that the value of  $\beta(R)$  at  $R = (R_c + 3 \text{ Å})$  equals  $\beta_{M}$ multiplied by a factor of 1.2, 1.1, 1.0, and 0.9, respectively. Also plotted in Fig. 6 (curve 1) is a Varshni potential for the ON-O stretch.<sup>23</sup> The latter is similar to the above modified Morse curve with the multiplication factor equal to 1.3. In Table IV Monte Carlo estimates,  $(N_{EJ}^{MC} \pm \sigma^{MC})/(2J+1)$ , based on the above choices for  $\beta\left(R\right)$ , are given for  $N_{EJ}$  for a low, medium, and high energy for each of three J values.  $N_{EI}^{MC}$  was calculated, now in R increments of 0.2 Å, to locate the transition state at  $R^{\dagger}$ . The  $R^{\dagger}$  values corresponding to the entries in Table IV are given in Table V.

While an interpolation function  $= \exp[-\alpha(q-q_e)]$ , where q is the reaction coordinate, has been assumed in the SACM treatment, 19 and also elsewhere to approximate transitional bending frequencies in a RRKM-type model,<sup>20</sup> recent ab initio calculations<sup>21</sup> on the CH<sub>4</sub>→CH<sub>3</sub> + H potential energy surface and subsequent analytical fitting<sup>24</sup> suggested an inadequacy of this interpolation for describing the quadratic force constant for a bending motion involving the angle between a C-H bond in CH<sub>3</sub> and C-H interfragment displacement vector. The sensitivity of the value of  $N_{EI}(R^{\dagger})$  to the form of the bending potential  $V_{\rm bend}$  for NO<sub>2</sub> $\rightarrow$ NO + O was tested next. In particular, the  $g^2$  in Eq. (A4) for  $V_{\text{bend}}$  was replaced by  $\frac{1}{3}(2g+g^2)$ , an interpolation reported to reproduce satisfactorily R-dependent eigenvalues for a particular 1D hindered rotor potential.<sup>25</sup> In Fig. 7 the values of g,  $g^2$ , and  $\frac{1}{3}(2g+g^2)$  are plotted vs  $(R - R_e)$  for  $\alpha = 1.3 \,\text{Å}^{-1}$ . The values of  $[N_{EI}^{MC}(R^{\dagger}) \pm \sigma^{MC}]$ /(2J+1) and  $R^{\dagger}$  for the two interpolations used for  $V_{\rm bend}$ ,  $g^2$ , and  $\frac{1}{3}(2g + g^2)$  are compared in Table VI.

TABLE IV. Dependence of  $N_{EJ}(R^{\dagger})$  on  $V_{bf}$  for  $NO_2 \rightarrow NO + O$ .

7	E' 2.29	•	[/	$[N_{EJ}^{ ext{MC}}(R^{\dagger}) \pm \sigma^{ ext{MC}}]/(2J+1)$			
$(\tilde{n}=1)$	$(\text{kcal mol}^{-1})$	1	2	3	4	5	
0	0 20 40	$8.5 \pm 0.1$ $160 \pm 1$ $457 \pm 1$	$9.7 \pm 0.1$ $167 \pm 1$ $469 \pm 2$	$10.7 \pm 0.1$ $178 \pm 1$ $484 \pm 2$	$11.8 \pm 0.1$ $191 \pm 1$ $504 \pm 2$	$   \begin{array}{c}     13.8 \pm 0.2 \\     203 \pm 1 \\     526 \pm 1   \end{array} $	
10	0 20 40	$ 124 \pm 2  2730 \pm 20  8220 \pm 30 $	$141 \pm 2$ $2860 \pm 20$ $8420 \pm 30$	$154 \pm 2$ $3060 \pm 20$ $8700 \pm 40$	$175 \pm 2$ $3310 \pm 20$ $8960 \pm 40$	$206 \pm 3$ $3540 \pm 20$ $9490 \pm 40$	
20	0 20 40	$139 \pm 2$ $4580 \pm 30$ $14600 \pm 100$	$   \begin{array}{c}     163 \pm 3 \\     48100 \pm 40 \\     15000 \pm 100   \end{array} $	$187 \pm 3$ $5150 \pm 40$ $15500 \pm 100$	$229 \pm 3$ $5600 \pm 40$ $16100 \pm 100$	$283 \pm 3$ $6050 \pm 30$ $16900 \pm 100$	

<sup>\*</sup>The columns labeled 1-5 refer to the use of the similarly numbered potential energy curves in Fig. 6 for the bond-fission potential  $V_{\rm bf}$ .

TABLE V. Dependence of  $R^{\dagger}$  on  $V_{bf}$  for  $NO_2 \rightarrow NO + O.$ <sup>a</sup>

J	$E_{\infty}' - 2.29$			$R^{\dagger}(\mathring{\mathbf{A}})$		
$(\hbar = 1)$	$(\text{kcal mol}^{-1})$	1	2	3	4	5
0	0	2.8	2.9	3.0	3.0	3.0
	20	2.4	2.4	2.4	2.5	2.6
,	40	2.4	2.4	2.4	2.5	2.5
10	0	2.9	3.0	3.0	3.0	3.0
	20	2.4	2.4	2.4	2.5	2.6
4.	40	2.4	2.4	2.4	2.4	2.4
20 -	0	3.0	3.0	3.0	3.0	3.1
	20	2.4	2.4	2.4	2.5	2.6
	40	2.3	2.3	2.3	2.4	2.4

<sup>\*</sup>The columns labeled 1-5 are defined in Table IV, Footnote a.

## V. SPECIFIC RATE CONSTANTS FOR ETHANE DECOMPOSITION

To assess further the practicality of the present method, microcanonical decomposition rate constants  $k_{EJ}$  [Eq. (1)] for  $C_2H_6\rightarrow 2CH_3$  were calculated as a function of energy for several J values. The numerator  $N_{EJ}(R^{\dagger})$  in Eq. (1) was taken to be minimum in  $N_{EJ}(R)$  on an equally spaced set of R values with  $\Delta R=0.1$  Å. The  $N_{EJ}(R)$  values were obtained from Eq. (E8) and the methods described in Sec. III and Appendix F. Further details, including  $R^{\dagger}$  values and an energy, and R-dependent restriction on the realtive orientation of the two methyl radicals, are given in Ref. 7. To obtain a simple yet realistic estimate of the density of states  $\rho_{EJ}$  in Eq. (1) a straightforward approach was adopted, yielding<sup>26</sup>

$$\rho_{EJ} = (2J+1)\rho_v(E'_r - J^2/2I_{A,r})F_\rho(E'_r,J)\sigma_r^{-1}, \qquad (12)$$

where  $\sigma_r$  is the symmetry number for the reactant. In Eq. (12) the total energy available to the reactant  $E'_r$  is  $E'_\infty$  plus the dissociation energy into the two methyl groups  $D_0(C-C)$ ,  $I_{A,r}$  is the moment of inertia perpendicular to the symmetry axis of  $C_2H_6$  with its equilibrium geometry, and  $F_\rho(E'_r,J)$  is a

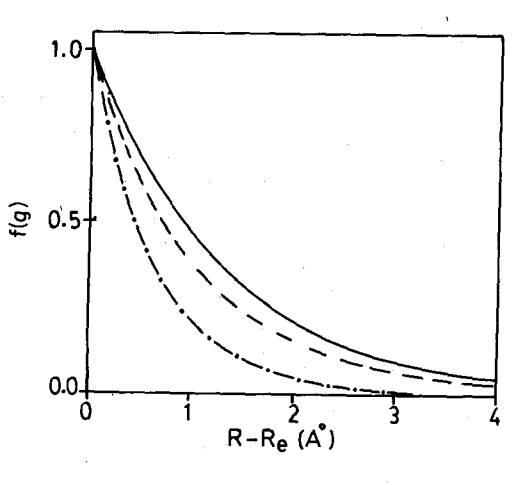


FIG. 7. Interpolation functions f(g) used to construct model potential energy surfaces for the NO<sub>2</sub> $\rightarrow$ NO + O system. Plotted vs  $(R-R_e)$  are  $g = \exp[-\alpha(R-R_e)]$  (—),  $\frac{1}{2}[2g+g^2]$  (—), and  $g^2$  (—). Here,  $\alpha = 1.3$  Å<sup>-1</sup> and  $R_e$  is the equilibrium value of R for NO<sub>2</sub>.

rotational correction factor given in Appendix I. For harmonic oscillators the density of vibrational states  $\rho_{v}$  is given, in the Whitten-Rabinovitch approximation,<sup>27</sup> by

$$\rho_{\nu}(x) = \left[x + a(x)E_{Zr}\right]^{s-1} / \left[\Gamma(s)\prod_{i=1}^{s}h\nu_{i}\right], \tag{13}$$

where  $x = E'_r - J^2/2I_{A,r}$ ,  $v_i$  is the frequency of the *i*th normal mode of  $C_2H_6$  (Tables IX and X),  $E_{Zr}$  is the zero point energy of the reactant, and s is the number of its oscillators. For ethane s = 18 when the torsional motion of the  $CH_3$  groups is treated as a vibration, as we shall do, for convenience in the present illustrative calculations. The parameter a(x) is a function defined by Whitten and Rabinovitch.  $^{27(b)}$ 

The rate constant expression is

$$k_{EJ} = N_{EJ}(R^{\dagger})/h(2J+1)\rho_{\nu}(x)F_{\rho}(x,J)\sigma_{r}^{-1}.$$
 (14)

For the present model of the reactant molecule,  $\sigma_r = 6$ . As discussed in Appendix E a value of  $\sigma = 72$  is used in the expression for  $N_{EJ}$  [Eq. (E8)] for the case of nearly loose transition states. Results for  $k_{EJ}$  vs  $E'_{\infty}$  for a wide range of J values are shown in Fig. 8. For each J the energy ranges from near threshold to  $E'_{\infty} \cong 63$  kcal mol<sup>-1</sup>.

#### VI. DISCUSSION

#### A. $NO_2 \rightarrow NO + O$

The values of  $N_{EJ}(R^{\dagger})$  calculated by the present method were seen in Sec. IV to be close to those at  $R = \infty$ ,  $N_{EJ}(\infty)$ . Thus, the transition state for the model potential is relatively loose. The values were also close to those calculated in Ref. 19, as is seen from Fig. 5, except at low energies, where small differences in the molecular properties of the surface would have the largest effect. Our experience was that the present method was computationally faster than SACM at J = 20 and 40, even for a molecular system as small as  $NO_2 \rightarrow NO + O$ , presumably because of the large number of reactant and product states which occur at these J's and  $E'_{\infty}$ 's. (The most probable thermal value of J for  $NO_2$  at 500 K is about 40.)

The dependence of  $N_{EJ}/(2J+1)$  on  $V_{\rm bf}$  is seen from Table IV to be relatively minor for the range of energies, J's and functions considered, particularly at  $E'_{\infty}=42.29$  kcal

TABLE VI. Dependence of  $N_{EJ}(R^{\dagger})$  and  $R^{\dagger}$  on  $V_{\rm bend}$  for  $NO_2 \rightarrow NO + O$ .

ī	$E'_{m} = 2.29$	$[N_{EJ}(R^{\dagger}) \pm \sigma^{MC}]/(2J+1)$		$R^{+}(\mathring{\mathbf{A}})$	
$(\hslash=1)$	$(\text{kcal mol}^{-1})$	g <sup>2</sup>	$\frac{1}{3}[2g+g^2]$	<b>g</b> <sup>2</sup>	$\frac{1}{3}[2g+g^2]$
0	0	11.8 ± 0.1	5.7 ± 0.1	3.0	3.2
	20	191 ± 1	$115\pm 1$	2.5	2.6
	40	$504 \pm 2$	$354 \pm 2$	2.4	2.4
10	0	$175 \pm 2$	89 ± 2	3.0	3.3
	20	$3310 \pm 20$	$1960 \pm 20$	2.5	2.6
	40	$8960 \pm 40$	$6370 \pm 40$	2.4	2.4
20	0	$229 \pm 3$	98 ± 3	3.0	3.4
	20	$5600 \pm 40$	$3410 \pm 30$	2.5	2.7
	40	$16100 \pm 100$	$11100 \pm 100$	2.4	2.4

 $m mol^{-1}$ . Such results are not unexpected. Because of the looseness of the transition state, the value of  $N_{EJ}$  is relatively insensitive to  $V_{\rm bf}$ . A significantly stronger dependence of the rate on  $V_{\rm bf}$  has been reported for a different bond-fission system. <sup>28</sup>

For all J values in Table VI the  $N_{EJ}$  values calculated from  $g^2$  exceed those calculated from  $\frac{1}{3}(2g+g^2)$  by a factor of roughly 2, a result understood by comparing the two forms of  $V_{\rm bend}$  in Fig. 7: The larger bending force frequency arising in the  $\frac{1}{3}(2g+g^2)$  interpolation yields a smaller  $\Omega_J(\epsilon)$  and hence a smaller value for  $N_{EJ}$ .

#### B. C<sub>2</sub>H<sub>6</sub>→2CH<sub>3</sub>

Since detailed results for this reaction will be given elsewhere and compared with experimental values as well as

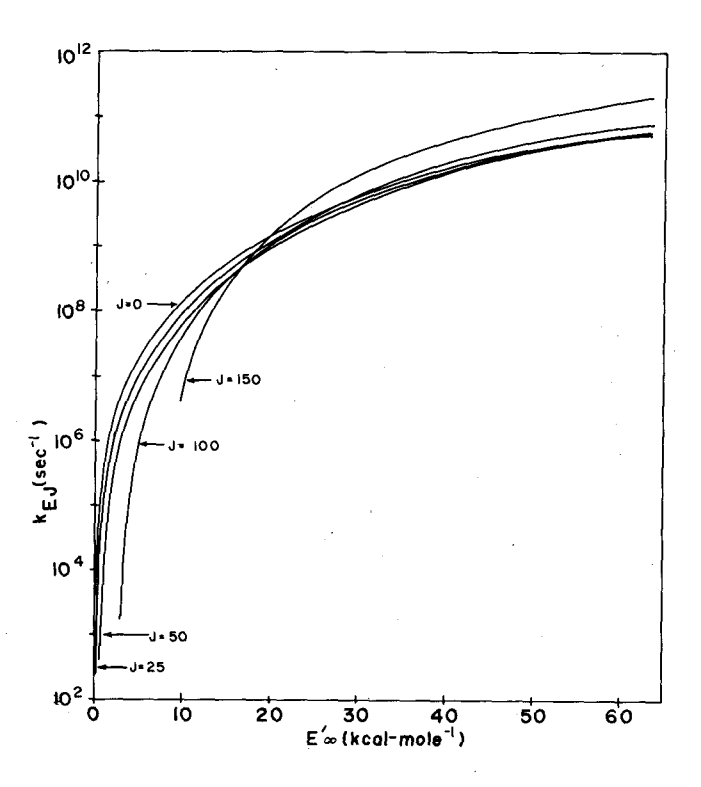


FIG. 8. Semilog plot of specific rate constants  $k_{EJ}$  vs  $E'_{\infty}$  for various values of J for the  $C_2H_6\rightarrow 2$  CH<sub>3</sub> reaction. The statistical uncertainty in the  $k_{EJ}$  values resulting from the Monte Carlo evaluation of  $N_{EJ}$  is, in general, too small to be resolved on the scale of the figure and has been omitted.

with other calculations, only several remarks are made here: It can be seen from Fig. 8 that the effective threshold energy increases with J, as expected from the centrifugal effect and in agreement with other work. (Actual determination of a threshold energy would require a quantum treatment for the zero point energy of the transition modes, a not too difficult task.) The energy dependence of the  $k_{EJ}$  curves in Fig. 8 is at least in qualitative agreement with that obtained elsewhere for a different model of the  $C_2H_6 \rightarrow 2CH_3$  system.

#### C. Quantum correction for transitional modes

The present method provides a practical method for calculating  $k_{EJ}$ 's for arbitrary potential energy surfaces. However, it can be anticipated that sufficiently near the threshold energy a quantum correction for the transitional modes will be necessary, particularly when the contribution of the cumulative density of states of those modes  $\int_0^{\epsilon} \Omega_r(x) dx$ (2J+1) for a typical  $\epsilon$  in Eq. (9) is comparable with unity. (There must be at least one quantum state in these transitional modes.) For the calculations in the present paper, this quantity always exceeded unity by an appreciable amount. We are currently extending the theory in this direction. A simple form of correction is the following: the value of  $N_{EJ}$  in Eq. (2) when  $\epsilon$  equals the zero point energy  $\epsilon_0$  of the transitional modes is usually  $(2J+1)N_{\nu}(E'-\epsilon_0)$ . This value can be connected by interpolation to values of  $N_{EI}$  given by Eq. (2) at somewhat higher energies. This correction would, by placing a lower limit on  $N_{EJ}$ , prevent the expression in Eq. (2) from becoming too small, i.e., less than (2J + 1), when E' becomes small enough that the system as a whole is in its ground state for the given value of the reaction coordinate.

#### VII. CONCLUSIONS

The above results show that the present method can be used to treat in a practical way unimolecular dissociations having transition states of arbitrary looseness. The dependence of results for the NO<sub>2</sub>→NO + O reaction on the potential energy function for bond fission and for bending was examined for a given set of model surfaces, with results given in Tables IV-VI. The present method can be used, however, with any potential energy surface. When a particular surface was chosen which led to molecular parameters having an

interpolation between those of reactants (NO2) and products (NO + O) analogous to the universal eigenvalue interpolation assumed in the SACM model, fairly similar results were obtained. The main attributes of the present method are its use of general potential energy functions and a computational feasibility which is unaffected by the size of the polyatomic fragments.

#### **ACKNOWLEDGMENTS**

It is a pleasure to acknowledge the support of this research by the National Science Foundation, USA, and (DMW) by a NSERC of Canada Postdoctoral Research Fellowship.

#### APPENDIX A: POTENTIAL ENERGY PARAMETERS AND COORDINATE TRANSFORMATION FOR NO₂→NO + O

For the reaction  $NO_2 \rightarrow NO + O$  a model potential  $V = V_c + V_t$  was used, where  $V_c$  denotes the NO bond potential (coordinate r) and  $V_t$  denotes the contribution to Varising from the angular coordinates and the ON-O separation distance [Eq. (A3)].  $V_c$  is taken to be a Morse potential function of r

$$V_c \equiv V_c(r;R)$$
=  $D(R)(1 - \exp\{-\beta(R)[r - r_e(R)]\})^2 - D(R)$ , (A1)

whose parameters  $D, \beta$ , and  $r_e$  themselves depend on R, the separation distance between the centers of mass of the two fragments. D(R) is a bond dissociation energy,  $\beta(R)$  a Morse parameter, and  $r_{e}(R)$  an equilibrium bond length at any giv-

Denoting D,  $\beta$ , and  $r_e^{-2}$  by X(R), an interpolation was used for these quantities,

$$X(R) = X_{O-N} - (X_{O-N} - X_{ON-O})g(R),$$

TABLE A1. Potential parameters for NO<sub>2</sub> system.

$g(R) = \exp$	$[-\alpha(R-R_e)],$		(A2)
---------------	---------------------	--	------

where  $R_{e}$  is the value of R at the equilibrium geometry of NO2. The subscripts ON-O and O-N indicate reactant and product quantities, respectively, for the NO bond. The form of the interpolation function g(R) is that proposed in Ref. 19. It was chosen here mainly to facilitate a comparison of the calculated  $N_{EJ}$  with the value for the statistical adiabaticchannel model of Ref. 19. However, in Ref. 19 a potential surface was not used but rather frequencies, moments of inertia, and angular momenta interpolated by g(R).

The transitional-mode potential  $V_t$  was taken to be

$$V_t = V_{\rm bf}(r_{\rm ON-O}) + V_{\rm bend}(\theta), \tag{A3}$$

where the bond-fission potential  $V_{\rm bf}$  is a Morse function, as in Eq. (A1) but with r replaced by  $r_{ON-O}$  and with D,  $\beta$ , and  $r_e$ being constants, namely the values for ON-O. The bending potential was modeled with a hindered rotor function,

$$V_{\text{bend}} = \frac{1}{2} f_{\theta} g^2(R) \sin^2(\theta - \theta_e), \tag{A4}$$

where  $f_{\theta}$  is a quadratic bending force constant and  $\theta_{e}$  is the equilibrium value of  $\theta$  in NO<sub>2</sub>. The  $g^2(R)$  factor makes the bending vibration frequency vary as g(R). The various coordinates used in Eqs. (A1)-(A4) are depicted in Fig. 1 and the relevant potential parameters are listed in Table A1.

In the text the internal coordinates were first converted to Jacobi coordinates and then the latter were expressed in terms of action-angle variables. The first transformation is made as follows: The three atoms lie in a plane, regarded as the body-fixed xy plane, and with an origin at the center of mass of the AB molecule. The coordinates are given in terms of r and  $\gamma$ :  $x_A = (\mu/m_A)r \cos \gamma$ ,  $y_A = (\mu/m_A)r \sin \gamma$ ;  $x_{\rm B} = -(\mu/m_{\rm B})r\cos\gamma$ ,  $y_{\rm B} = -(\mu/m_{\rm B})r\cos\gamma$ ,  $x_{\rm C} = R$ ,  $y_{\rm C} = 0$ . The BC bond distance,  $r_{\rm AB-C}$ , and the ABC bond angle  $\theta$  are readily expressed in terms of these coordinates.

Parameter	Value	Reference	Parameter	Value	Reference
		NO <sub>2</sub>			
$r_{\text{ON-O},e}$	1.1934 Å	30	$R_e$	1.699 Å	а
$\theta_e$	134.07°	30	$D_{\text{ON-O}}$	74.5 kcal mol <sup>-1</sup>	b
$v_1$	1356.9 cm <sup>-1</sup>	30	$\beta_{ON-O}$	3.266 Å <sup>-1</sup>	c
$v_2$	754.1 cm <sup>-1</sup>	30	$f_{ heta}$	$1.579 \times 10^{-11}  \mathrm{erg}$	d
$\nu_3$	1665.6 cm <sup>-1</sup>	30	$I_{Ae}$	$2.10$ amu Å $^2$	a
	$11.04 \times 10^5  \mathrm{erg}  \mathrm{cm}^{-2}$	30	$I_{\mathrm{Be}}$	$38.62 \text{ amu } \text{Å}^2$	a
$f_{rr} \ f_{aa}$	$1.109 \times 10^5 \mathrm{erg}\mathrm{cm}^{-2}$	30	$I_{\mathbf{C}_{e}}$	$40.73 \text{ amu Å}^2$	a
$D_0(ON-O)$	3.114 eV	. 31			
,		NO			
P	1.1508 Å	32	$D_{ON}$	$152.6 \text{ kcal mol}^{-1}$	ъ
r <sub>NO, e</sub> v	1903.6 cm <sup>-1</sup>	32	$\beta_{\rm ON}^{\rm e}$	$2.742 \text{ Å}^{-1}$	c
$D_0(NO)$	6.5 eV	32	, on		
α	$1.3^{\circ} \text{Å}^{-1}$	19 <sup>f</sup>			

<sup>&</sup>lt;sup>a</sup> Determined by  $r_{ON-O, e}$  and atomic masses.

 $<sup>^{</sup>b}D_{\text{ON-O}} = D_{0}(\text{ON-O}) + E_{zr} - E_{zp} \text{ and } D_{\text{ON}} = D_{0}(\text{ON}) + E_{zp}; E_{zr} = (2\pi/2)(\nu_{1} + \nu_{2} + \nu_{3}) \text{ and } E_{zp} = (2\pi/2)\nu_{1}$ 

 $<sup>^{\</sup>circ}B_{\text{ON-O}} = [f_{rr}/2D_{\text{ON-O}}]^{1/2}$ , where  $f_{rr}$  is the diagonal quadratic stretching force constant for NO<sub>2</sub>.

 $<sup>{}^{\</sup>circ} f_{\theta} \equiv f_{aa} [r_{\text{ON-O}, e}]^2$  where  $f_{aa}$  is the diagonal quadratic bending force constant for NO<sub>2</sub>.  ${}^{\circ} f_{\text{ON}} = 2\pi v [\mu/2D_{\text{ON}}]^{1/2}$ .

<sup>&</sup>lt;sup>f</sup>This value was found to provide a good fit of the statistical adiabatic-channel model to high-pressure thermal rate constant data (Ref. 19).

## APPENDIX B: POTENTIAL ENERGY PARAMETERS FOR $H_2O_2 \rightarrow 2OH$

For the reaction  $H_2O_2\rightarrow 2OH$  a model potential  $V=V_{c1}+V_{c2}+V_t$  analogous to that described in Appendix A was used. Each  $V_{ci}$  denotes an OH bond potential with coordinate  $r_i(i=1,2)$ , similar to Eq. (A1) with r now replaced by  $r_i$ . Denoting  $D, \beta$ , and  $r_e^{-2}$  by X(R), the interpolation used was again given by Eq. (A2), with ON-O and O-N subscripts replaced by HOO-H and O-H to indicate the values for the OH bond in the reactant and separated products, respectively. The transitional mode potential  $V_t$  was modeled by

$$V_{t} = V_{\rm bf}(r_{\rm HO-OH}) + V_{b1}(\theta_{1}) + V_{b2}(\theta_{2}) + V_{\tau}(\tau, \theta_{1}, \theta_{2}). \tag{B1}$$

The bond-fission potential  $V_{bf}$  was again taken to be a Morse function, as in Eq. (A1), with r, D,  $\beta$ , and  $r_e$  being the values for HO-OH, the latter three now being constants. The bending potentials  $V_{bi}(i=1,2)$  were chosen to be hindered rotor functions similar to that in Eq. (A4), but now with i subscripts added to the  $\theta$ 's and with  $\theta_{i,e}$  being the equilibrium H-O-O bond angle in  $H_2O_2$  (i=1,2). The torsional potential  $V_r$  in Eq. (B1) is a hindered rotor function, modified by

coupling to the bending modes. It is typically small in the coordinate domain of interest:

$$V_{\tau} = [V_0 + V_1 \cos \Delta \tau + V_2 \cos 2\Delta \tau + V_3 \cos 3\Delta \tau] \times \sin \theta_1 \sin \theta_2 g(R), \tag{B2}$$

where  $\Delta \tau = \tau - \tau_e$  and  $\tau_e$  is the equilibrium value of the torsional angle  $\tau$  in  $H_2O_2$ . The  $\sin\theta_1\sin\theta_2$  factor varies between 0 and 1, since  $0 \le \theta_i \le \pi$ , and ensures that the torsional potential is physically reasonable when  $\theta_i$  tends to 0 or  $\pi$ . The change in the equilibrium properties of  $H_2O_2$  introduced by this factor proved to be minor since  $\theta_{1,e}$  and  $\theta_{2,e}$  are close to  $\pi/2$  for  $H_2O_2$ . The g(R) interpolation used in Eq. (B2) for the torsional potential, namely that given by Eq. (A2), is somewhat similar to that used in Ref. 33 for a 1D hindered rotation about a threefold symmetry axis. The various coordinates used in the above equations are depicted in Fig. 3. The relevant potential parameters are listed in Table B1.

## APPENDIX C: POTENTIAL ENERGY PARAMETERS FOR $C_2H_6 \rightarrow 2CH_3$

For this larger system a model potential  $V = V_c + V_t$  was used, where  $V_t$ , the potential energy function for variation of the separation distance and orientation of the CH<sub>3</sub>

TABLE B1. Potential parameters for H2O2 system.

Value	Reference	Parameter	Value	Reference
	H <sub>2</sub> O	)2	,	
0.965 Å	34	$R_e$	1.485 Å	ь
1.462 Å	34	$D_{\text{HO-OH}}$	$54.6 \text{ kcal mol}^{-1}$	c
	34	$D_{\text{HOO-H}}$	95.8 kcal mol <sup>-1</sup>	c
	34		2.388 Å <sup>-1</sup>	d
	35		$2.453 \text{ Å}^{-1}$	đ
1402 cm <sup>-1</sup>	35	$f_{\theta}$ , $f_{\theta}$	$1.26 \times 10^{-11} \text{ erg}$	e
877 cm <sup>-1</sup>	35	$V_0$	$876.3 \text{ cm}^{-1}$	38 <sup>f</sup>
243 cm <sup>-1</sup>	35	$V_1$	$1093.4 \text{ cm}^{-1}$	38 <sup>f</sup>
3608 cm <sup>-1</sup>	35	$V_2$	$546.7 \text{ cm}^{-1}$	38 <sup>f</sup>
1266 cm <sup>-1</sup>	35	$V_3$	$-56.4  \mathrm{cm}^{-1}$	38 <sup>f</sup>
	36ª			
$8.009 \times 10^5  \mathrm{erg  cm^{-2}}$	36ª			
$0.894 \times 10^{5}  \mathrm{erg  cm^{-2}}$	36ª			
49.5 kcal $mol^{-1}$	37		i	•
$88.5 \text{ kcal mol}^{-1}$	37			
	HC	)2		
3410 cm <sup>-1</sup>	39			
1095 cm <sup>-1</sup>	39			
1390 cm <sup>-1</sup>	39	÷		
	O	Н		
0.9710 Å	40	$D_{OH}$	105.6 kcal mol <sup>-1</sup>	c
3735 cm <sup>-1</sup>	40		$2.285 \ { m \AA}^{-1}$	g
4.35 eV	40			
$1.0 \text{ Å}^{-1}$	h			
	0.965 Å 1.462 Å 100° 120° 3599 cm <sup>-1</sup> 1402 cm <sup>-1</sup> 877 cm <sup>-1</sup> 243 cm <sup>-1</sup> 3608 cm <sup>-1</sup> 1266 cm <sup>-1</sup> 4.322×10 <sup>5</sup> erg cm <sup>-2</sup> 8.009×10 <sup>5</sup> erg cm <sup>-2</sup> 0.894×10 <sup>5</sup> erg cm <sup>-2</sup> 49.5 kcal mol <sup>-1</sup> 88.5 kcal mol <sup>-1</sup> 3410 cm <sup>-1</sup> 1095 cm <sup>-1</sup> 1390 cm <sup>-1</sup> 0.9710 Å 3735 cm <sup>-1</sup> 4.35 eV	$\begin{array}{cccccccccccccccccccccccccccccccccccc$	$\begin{array}{c ccccccccccccccccccccccccccccccccccc$	$\begin{array}{c ccccccccccccccccccccccccccccccccccc$

<sup>&</sup>lt;sup>a</sup> The harmonic stretching force constants  $f_{RR}$  and  $f_{rr}$  for O-O and O-H, respectively, as well as the harmonic H-O-O bending force constant  $f_{aa}$  are *ab initio*/empirical values taken from Table 1 of Ref. 36.

<sup>&</sup>lt;sup>b</sup> Determined by given equilibrium geometry and atomic masses of H<sub>2</sub>O<sub>2</sub>.

 $<sup>{}^{\</sup>circ}D_{\text{HO-OH}} = D_0(\text{HO-OH}) + E_{zr} - 2E_{zp}; D_{\text{HOO-H}} = D_0(\text{HOO-H}) + E_{zr} - E_z'; D_{\text{OH}} = D_0(\text{OH}) + E_{zp}; \text{ where } (\text{with } \tilde{R} = 1) E_{zr} = (2\pi/2) \sum_{i=1}^{3} \nu_i, E_z' = (2\pi/2) \sum_{i=1}^{3} \nu_i', \text{ and } E_{zp} = (2\pi/2)\nu.$ 

 $<sup>{}^{</sup>d}\beta_{\text{HO-OH}} = [f_{RR}/2D_{\text{HO-OH}}]^{1/2}, \beta_{\text{HOO-H}} = [f_{rr}/2D_{\text{HOO-H}}]^{1/2}.$ 

 $<sup>{}^{</sup>c}f_{\theta_{i}} = f_{aa} [r_{\text{HOO-H, }e}] [r_{\text{HO-OH, }e}] (i = 1, 2).$ 

<sup>&</sup>lt;sup>f</sup>Our values of  $V_0$ ,  $V_1$ ,  $V_2$ ,  $V_3$  are determined by the experimental barrier heights reported in Ref. 38 and by requiring  $V_{\tau}(0) = \partial V_{\tau}(0)/\partial \tau = 0$ .

 $<sup>^{8}</sup>eta_{\mathrm{OH}} = 2\pi\nu(\mu_{\mathrm{OH}}/2D_{\mathrm{OH}})^{1/2}.$ 

<sup>&</sup>lt;sup>h</sup> In Ref. 19,  $\alpha$  was obtained by fitting to thermal rate constant data. In the absence of such fits for  $H_2O_2$ , we adopt the "standard" value (Refs. 19 and 41) of  $\alpha = 1.0 \text{ Å}^{-1}$ .

TABLE C1. Correlation of conserved vibrations.<sup>a</sup>

Label i	Mode	C <sub>2</sub> H <sub>6</sub> Symmetry type	ν	$ar{oldsymbol{v}}_{ir}$	Mode	CH <sub>3</sub> Symmetry type	$ u_{ip}$
1	$\nu_1$	A 18	2954	2925.0	$\nu_{\rm l}$	A '1	3044
	$\nu_{5}$	$A_{2u}$	2896				
2	$v_2$	$A_{1g}$	1388	1383.5	$ u_2$	A "	580
	$\nu_6$	A 2u	1379				
3	$\nu_7$	$\boldsymbol{E_u}$	2985	2977.0	$\nu_3$	E'	3162
	$\nu_{10}$	$E_{g}$	2969	•			
4	$ u_8$	$egin{array}{c} E_g \ E_u \end{array}$	1472	1470.5	$ u_4$	E'	1396
	$ u_{11}$	$E_{g}$	1469				

<sup>&</sup>lt;sup>a</sup> All frequencies are in units of cm<sup>-1</sup> and are taken from Ref. 19.

groups, is given later in Eq. (C3). The potential  $V_c$  for the "conserved" vibrational degrees of freedom (listed in Table C1) was assumed for simplicity to be separable and quadratic. Their vibrational energy in excess of the zero point energy was then expressed in terms of principal quantum numbers  $n_{i1}$  and  $n_{i2}$  of normal modes in methyl fragments 1 and 2:

$$E'_{V} = \sum_{i=1}^{4} 2\pi v_{i}(R) [n_{i1} + n_{i2}].$$
 (C1)

The sum is over the (identical) vibrations of each methyl group, two of which are doubly degenerate. The frequencies  $v_i(R)$  were obtained by interpolation:

$$v_i(R) = v_{ip} + (\bar{v}_{ir} - v_{ip})g(R)[i = 1,...,4],$$
 (C2)

where R is the separation distance between the centers of mass of the methyl fragments and g is given by Eq. (A2). The product frequencies  $v_{ip}$  are the normal mode frequencies of an isolated methyl radical and are listed with their symmetry type in Table C1. The reactant's frequencies  $\bar{v}_{ir}$ , which correlate to the  $v_{ip}$  via Eq. (C2), were determined as follows: For a given symmetry type (either A or E) and for each type of vibration (either CH<sub>3</sub> stretching or CH<sub>3</sub> deformation) two nearly degenerate frequencies were averaged. The resultant  $\bar{v}_{ir}$ 's were then correlated on a 1:1 basis with the  $v_{ip}$ 's according to symmetry type and characteristic vibrational motion of symmetry type and characteristic vibrational motion and are listed in Table C1, together with their symmetry type. The remaining normal vibrational modes of  $C_2H_6$  become transitional modes as R increases and are listed in Table C2.

The potential  $V_t$  for the "transitional" degrees of freedom and for the bond-fission coordinate  $r_{CC}$  is assumed to arise from nonbonded and bonded interactions,

$$V_t = V_{\rm NB} + V_{\rm B},\tag{C3}$$

described below.

TABLE C2. Disappearing vibrational modes of C<sub>2</sub>H<sub>6</sub>.<sup>a</sup>

Mode	Symmetry type	ν	Description
$\nu_3$	A 10	995	C-C stretch
$v_4$	$A_{1g} \\ A_{1u}$	289	torsion
$\nu_9$	$E_u^{\prime u}$	821	CH <sub>3</sub> rock
$\nu_{12}$	$E_{g}^{u}$	1206	CH <sub>3</sub> rock

<sup>&</sup>lt;sup>a</sup> All frequencies are in cm<sup>-1</sup> and are taken from Ref. 19.

#### 1. Nonbonded interaction $V_{\rm NB}$

Between all nonbonded H···H and C···H pairs a Lennard-Jones potential  $V_{\rm LJ}$ , given by  $\epsilon[(r_0/r)^{12}-2(r_0/r)^6]$ , was used and Coulomb interactions arising from residual point charges on different atoms were neglected.<sup>42</sup> The resultant nonbonded potential is

$$V_{\rm NB} = \sum_{i,j=1}^{4} V_{\rm LJ}(r_{ij}),$$
 (C4)

where i and j label atoms on different CH<sub>3</sub> fragments and the prime indicates that the C···C contribution is excluded. The parameters for the various  $V_{LJ}$ 's are listed in Table C3.

#### 2. Bonded interaction $V_{\rm B}$

For the C···C bond-fission potential a Morse function was used, modified by an orientational factor to include in an approximate way the influence of the now-bent C···C bond<sup>43</sup>:

$$V_{\rm B} = V_{\rm M}^{\rm eff}(r_{\rm CC})\cos^2\theta_1\cos^2\theta_2, \tag{C5}$$

where an effective potential  $V_{M}^{eff}$  was introduced:

$$V_{\rm M}^{\rm eff} = D_{\rm CC}^{\rm eff} \left\{ 1 - \exp\left[ -\beta_{\rm CC}^{\rm eff} (r_{\rm CC} - r_{\rm CC,e}^{\rm eff}) \right] \right\}^2 - D_{\rm CC}^{\rm eff}.$$
 (C6)

Here,  $r_{\rm CC}(=|\mathbf{r}_{\rm CC}|)$  is the carbon-carbon separation distance and  $\theta_i$  is the angle between  $\mathbf{r}_{\rm CC}$  and the symmetry axis of  $(\mathrm{CH}_3)_i (i=1,2)$ .

The effective Morse parameters in Eq. (C6) were determined by a least-squares fit of a known C-C Morse function  $V_{\rm M}$  to the sum of the potentials  $V_{\rm NB}+V_{\rm B}$  given by Eqs. (C3) to (C6) and evaluated along the minimum energy path from reactant to products. The latter was obtained by constraining the CH<sub>3</sub> groups to be in the same relative orientation as in equilibrium  $C_2H_6[\theta_1=0,\,\theta_2=\pi$  in Eq. (C5)] and by using the interpolated R-dependent CH<sub>3</sub> structure described below. A least-squares fit over the  $r_{\rm CC}$  interval of 1.75 to 6.78 Å yielded a  $V_{\rm M}^{\rm eff}$  with a root-mean-square deviation of 0.35 kcal mol<sup>-1</sup> from  $V_{\rm M}$ . The largest deviations occurred in the 1.75 to 2.1 Å interval, a region for which the potential was not needed. In the region of particular interest, namely,  $r_{\rm CC} \gtrsim 2.2$  Å,  $V_{\rm M}^{\rm eff}$  was slightly less negative than  $V_{\rm M}$ .

In order that the structure of each  $CH_3$  group evolved smoothly when R was varied, from that in  $C_2H_6$  to that of an isolated methyl radical, the local equilibrium carbon-hydrogen bond length  $r_{CH}$  and the H-C-H bond angle  $\alpha_{HCH}$  were

TABLE C3. Potential parameters for C<sub>2</sub>H<sub>6</sub> system.

Parameter	Value	Reference	Parameter	Value	Reference
-		C <sub>2</sub> H <sub>6</sub>			
r <sub>CH, e</sub>	1.111 Å	34	$R_e$	1.696 Å	b
r <sub>CC.e</sub>	1.533 Å	34	$D_{CC}$	96.6 kcal mol <sup>-1</sup>	c
$\alpha_{\text{HCH, e}}$	107.3°	34	$oldsymbol{eta_{cc}}$	$1.80  { m \AA}^{-1}$	d
$\beta_{\text{HCC, e}}$	111.4°	34	$D_{ m CC}^{ m eff}$	202.5 kcal mol <sup>-1</sup>	e
$ au_e$	60°	34	$oldsymbol{eta}_{ ext{CC}}^{ ext{eff}}$	1.90 Å <sup>−1</sup>	е
$f_{ m cc}$	$4.342 \times 10^{5}  \mathrm{erg \ cm^{-2}}$	44	$r_{CC,e}^{eff}$	1.175 Å	e
$D_0(C-C)$	87.60 kcal mol <sup>-1</sup>	34ª			
		CH <sub>3</sub>			
r <sub>CH, e</sub>	1.079 Å	31	$a_{ ext{HCH, e}}$	120°	31
		$CH_3 \cdots CH_3$			
$\epsilon_{\mathrm{H} \dots \mathrm{H}}$	$0.010 \mathrm{kcal} \mathrm{mol}^{-1}$	43	r <sub>H···H</sub> , o	3.37 Å	43
$\epsilon_{\mathrm{CC}}$	$0.095 \text{ kcal mol}^{-1}$	43	$r_{\text{C}}$	3.88 Å	43
$\epsilon_{ ext{c-H}}$	$0.031 \text{ kcal mol}^{-1}$	e	$r_{\text{C} \cdot \cdot \cdot \text{H, O}}$	3.62 Å	f
α	$1.0 \ { m \AA}^{-1}$	g			

<sup>&</sup>lt;sup>a</sup> Experimental value.

obtained at each R by an interpolation:

$$r_{\text{CH}}(R) = r_{\text{CH},e}^{p} + \left[r_{\text{CH},e}^{r} - r_{\text{CH},e}^{p}\right]g(R),$$

$$\alpha_{\text{HCH}}(R) = \alpha_{\text{HCH},e}^{p} + \left[\alpha_{\text{HCH},e}^{r} - \alpha_{\text{HCH},e}^{p}\right]g(R). \tag{C7}$$

Here, the superscripts p and r denote product (isolated  $CH_3$ ) and reactant ( $C_2H_6$ ) quantities, respectively. The  $CH_3$  structure, and the relative separation and orientation of the two  $CH_3$  groups together determined the interfragment atomic separations and hence the  $V_t$  in Eq. (C3). In addition, the  $CH_3$  structure determined the three moments of inertia,  $I_A(R)$ ,  $I_B(R)$ , and  $I_C(R)$ , used to assign a (rigid-rotor) rotational energy to each fragment.

The parameters appearing in Eqs. (C4)–(C7) as well as other relevant parameters are listed in Table C3. In Fig. 4(b) the various bond angles and bond distances that determined  $V_t$ , are depicted. When the actual potential energy surface is available no interpolation function g(R) is needed.

# APPENDIX D: ACTION-ANGLE AND INTERNAL COORDINATES AND DENSITY OF STATES FOR NONLINEAR SYSTEMS ABCD—AB + CD, SUCH AS $H_2O_2$ —2 OH

For these systems the canonically conjugate set of action-angle variables which specifies the space-fixed orientations and angular momenta of all four atoms is  $(j_1, j_{1z}, j_2, j_{2z}, l, l_z, \alpha_1, \beta_1, \alpha_2, \beta_2, \alpha_1, \beta_1)$ . The variables  $j_1$  and  $j_2$  are the individual rotational angular momentum actions of fragments 1 and 2 (i.e., the linear species AB and CD, respectively),  $j_{1z}$  and  $j_{2z}$  are their space-fixed z components, and l and  $l_z$  are as described in Sec. II. Instead of  $(j_{1z}, j_{2z}, l_z)$  and their

conjugate angles  $(\beta_1, \beta_2, \beta_1)$  it is convenient to use  $(k, J, J_z)$  and their angles  $(\alpha_k, \alpha, \beta)$ , where k is an intermediate angular momentum action associated with a vector sum  $|\mathbf{j}_1 + \mathbf{j}_2|$ ,  $\alpha_k$  is its conjugate angle, and  $(J, J_z, \alpha, \beta)$  are as defined before. For systems described by the above variables and for any given value of J we now have

$$\Omega_{J}(\epsilon) = (2\pi)^{-6}\sigma^{-1}\int \cdots \int \\ \times dJ_{z} dj_{1} dj_{2} dk dl d\alpha d\beta d\alpha_{1} d\alpha_{2} d\alpha_{k} d\alpha_{l} \\ \times \Delta (J, k, l)\Delta (k, j_{1}, j_{2})\delta(\epsilon - H_{cl}).$$
 (D1)

The  $\Delta$  functions and the integration limits are similar to those described for Eq. (4).  $H_{\rm cl}$  is written as

$$H_{\rm cl} = \frac{j_1^2}{2\mu_1 r_1^2} + \frac{j_2^2}{2\mu_2 r_2^2} + \frac{l^2}{2\mu R^2} + V_t(r_{\rm AB-CD}, \theta_1, \theta_2, \tau), \tag{D2}$$

where  $\mu_i$  is the reduced mass of fragment i, and  $\mu$  is the reduced mass for the relative motion of the AB and CD fragments. The potential  $V_t$  is modeled to be a function of the internal coordinates  $r_{\text{AB-CD}}$  (the BC distance),  $\theta_1$ ,  $\theta_2$ , and  $\tau$  depicted in Fig. 3(a) using  $H_2O_2$  as an example. The remaining two coordinates in Fig. 3(a) describe AB and CD vibrations and so are included in  $N_V(E'-\epsilon)$ . The reaction coordinate R, the angular momenta  $j_1$ ,  $j_2$ , and l, the angles  $\gamma_i$  between  $\mathbf{R}$  and  $\mathbf{r}_i$  (i=1,2), and the angle  $\lambda$  between  $\mathbf{r}_1 \times \mathbf{R}$  and  $\mathbf{r}_2 \times \mathbf{R}$  are depicted in Fig. 3(b).  $V_t$  is described in Appendix  $\mathbf{P}$ 

To evaluate the  $V_t$  in Eq. (D2), the internal coordinates  $r_{AB-CD}$ ,  $\theta_1$ ,  $\theta_2$ , and  $\tau$  are first expressed in terms of the Jacobi

<sup>&</sup>lt;sup>b</sup> Determined by given equilibrium geometry and atomic masses of C<sub>2</sub>H<sub>6</sub>.

 $<sup>^{</sup>c}D_{CC} = D_{0}(C-C) + E_{zr} - E_{zp}$  where  $E_{zr}$  and  $E_{zp}$  are determined by the normal mode frequencies of  $C_{2}H_{6}$  and  $CH_{3}$ , respectively, as listed in Tables C1 and C2.

 $<sup>{}^{\</sup>rm d}\boldsymbol{\beta}_{\rm CC} = (f_{\rm CC}/2D_{\rm CC})^{1/2}$ 

Obtained by least squares fitting as outlined in Appendix C.

 $<sup>^{\</sup>mathrm{f}}\epsilon_{\mathrm{C}\cdots\mathrm{H}} = (\epsilon_{\mathrm{H}\cdots\mathrm{H}}\epsilon_{\mathrm{C}\cdots\mathrm{C}})^{1/2}; r_{\mathrm{C}\cdots\mathrm{H,O}} = \frac{1}{2}(r_{\mathrm{H}\cdots\mathrm{H,O}} + r_{\mathrm{C}\cdots\mathrm{C,O}}).$ 

<sup>&</sup>lt;sup>8</sup> The standard value (Refs. 19 and 41) of  $\alpha = 1.0 \, \text{Å}^{-1}$  is adopted. A value of  $\alpha = 0.82 \, \text{Å}^{-1}$  has been used in an earlier work (Ref. 20).

coordinates  $(R, r_1, r_2, \gamma_1, \gamma_2, \lambda)$ , as in the final paragraph of this Appendix. For any R the values of  $r_1$  and  $r_2$  are then replaced by R-dependent equilibrium values  $r_e$  (Appendix B). The angles  $\lambda$ ,  $\gamma_1$ , and  $\gamma_2$  are next written as functions of J,  $j_1, j_2, k, l, \alpha_1, \alpha_2, \alpha_k$ , and  $\alpha_l$ , with the aid of the following expressions obtained from Eq. (7), with a, b, c, and d identified in Table III:

$$\cos \varphi = \cos \gamma_1 \cos \gamma_2 + \sin \gamma_1 \sin \gamma_2 \cos \lambda, \qquad (D3)$$

$$\cos \gamma_i = (\cos \theta_R \cos \theta_{ri} + \sin \alpha_i \sin \alpha_l \cos \theta_{li})/\cos \alpha_k, \qquad (D4)$$

where

$$\cos \varphi = \cos \alpha_1 \cos \alpha_2 + \sin \alpha_1 \sin \alpha_2 \cos \theta_{12}, \qquad (D5)$$

$$\cos \theta_R = \cos \alpha_k \cos \alpha_l + \sin \alpha_k \sin \alpha_l \cos \theta_{lk}, \quad (D6)$$

and

$$\cos \theta_{ri} = \cos \alpha_k \cos \alpha_i - \sin \alpha_k \sin \alpha_i \cos \theta_{ki}. \quad (D7)$$

In these equations  $\varphi$  is the angle between the vectors  $\mathbf{r}_1$  and  $\mathbf{r}_2$ ,  $\theta_R$  is the angle between the vectors  $\mathbf{R}$  and  $\mathbf{j}_1 \times \mathbf{j}_2$ , and  $\theta_{\kappa i}$  is the angle between  $1 \times \mathbf{k}$  and  $\mathbf{r}_i$  (i = 1, 2). The cosines of various other angles in the above equations are given in terms of the desired variables in Tables I and II.  $H_{\rm cl}$  is now seen to be completely specified by the variables  $(R, r_1, r_2, J, j_1, j_2, k, l, \alpha_1, \alpha_2, \alpha_k, \alpha_l)$  and to be independent of  $(J_z, \alpha, \beta)$ . Equation (D1) thus becomes

$$\Omega_{J}(\epsilon) = (2J+1)(2\pi)^{-4}\sigma^{-1}\int \cdots \int \\ \times dj_{1} dj_{2} dk dl d\alpha_{1} d\alpha_{2} d\alpha_{k} da_{l} \\ \times \Delta (J, k, l)\Delta (k, j_{1}, j_{2})\delta(\epsilon - H_{cl}),$$
 (D8)

which, combined with Eq. (2), yields the analog of Eq. (9),

$$N_{EJ} = (2J+1)(2\pi)^{-4}\sigma^{-1}\int \cdots \int \\ \times dj_1 \, dj_2 \, dk \, dl \, d\alpha_1 \, d\alpha_2 \, d\alpha_k \, d\alpha_l \\ \times N_V(E'-H_{cl})\Delta \, (J,k,l)\Delta \, (k,j_1,j_2).$$
 (D9)

The evaluation of the integral in Eq. (D9) is described in Sec. III. For the particular case of  $H_2O_2$ ,  $\sigma$  is 2. (In the case of the calculations of  $N_{EJ}$  in part I for  $H_2O_2$  only the integral was given and not the  $\sigma^{-1}$  contribution.)

The coordinate transformation referred to earlier from internal to Jacobi coordinates is readily made. The AB fragment is chosen to lie in the body-fixed xy plane and the center of mass of CD to lie on the positive x axis. The coordinates of the various atoms then are as follows:

$$\begin{aligned} x_{\rm A} &= (\mu_{\rm AB}/m_{\rm A})r_1\cos\gamma_1, \\ y_{\rm A} &= (\mu_{\rm AB}/m_{\rm A})r_1\sin\gamma_1, \\ z_{\rm A} &= z_{\rm B} = 0, \\ x_{\rm B} &= -(\mu_{\rm AB}/m_{\rm B})r_1\cos\gamma_1, \\ y_{\rm B} &= -(\mu_{\rm AB}/m_{\rm B})r_1\sin\gamma_1, \\ x_{\rm C} &= -(\mu_{\rm CD}/m_{\rm C})r^2\cos\gamma_2 + R, \\ y_{\rm C} &= -(\mu_{\rm CD}/m_{\rm C})r^2\sin\gamma_2\cos\lambda + R, \\ z_{\rm C} &= -(\mu_{\rm CD}/m_{\rm C})r_2\sin\gamma_2\sin\lambda + R, \\ x_{\rm D} &= (\mu_{\rm CD}/m_{\rm D})r_2\cos\gamma_2 + R, \\ y_{\rm D} &= (\mu_{\rm CD}/m_{\rm D})r_2\sin\gamma_2\cos\lambda + R, \\ z_{\rm D} &= (\mu_{\rm CD}/m_{\rm D})r_2\sin\gamma_2\sin\lambda + R, \end{aligned}$$

where  $\mu_{AB}$  is the reduced mass of A and B. The internal coordinates for the transitional modes, namely the BC bond length,  $r_{AB-CD}$ , the bond angles  $\theta_1$ ,  $\theta_2$ , and  $\tau$  are readily expressed in terms of these coordinates, e.g.,  $\cos \theta_i = \mathbf{e}_i \cdot \mathbf{e}_{AB-CD}$  and  $\cos \tau = (\mathbf{e}_1 \times \mathbf{e}_{AB-CD}) \cdot (\mathbf{e}_2 \times \mathbf{e}_{AB-CD}) / \sin \theta_1 \sin \theta_2$ , where  $\mathbf{e}_i$  and  $\mathbf{e}_{AB-CD}$  denote unit vectors along  $\mathbf{r}_i$  and  $\mathbf{r}_{AB-CD}$ , respectively.

#### APPENDIX E: ACTION-ANGLE COORDINATES, INTERNAL COORDINATES, AND DENSITY OF STATES FOR DISSOCIATION INTO POLYATOMIC FRAGMENTS

The material in this Appendix is grouped into four parts: In (1) a set of action-angle variables suited to polyatomic fragments is obtained. In (2) the density of transitional states  $\Omega_J(\epsilon)$  and the classical Hamiltonian  $H_{\rm cl}$  for the transitional modes are expressed in terms of these variables. Since the potential energy contribution to  $H_{\rm cl}$  is modeled in this study to be a function of interfragment atomic separation distances as well as two bond angles, a transformation from the action-angle variables to these internal coordinates is given in (3). Part (4) describes the minor modifications to (2) required to treat asymmetric rather then symmetric top fragments.

#### 1. Coordinates

For this polyatomic case, written as  $X_1X_2 \rightarrow X_1 + X_2$ , such as  $C_2H_6 \rightarrow 2$  CH<sub>3</sub>, the following system of coordinates, applicable to systems with nonlinear polyatomic fragments, was introduced. We let (x, y, z) denote a set of Cartesian coordinate axes fixed in the  $X_1 \cdots X_2$  system, the z axis being chosen to lie along the relative orbital angular momentum action vector  $\mathbf{l}$  of the fragments, as in Fig. 4(a). The x axis is chosen to lie along a vector  $\mathbf{l} \times \mathbf{k}$ , where  $\mathbf{k}$  is defined to be  $\mathbf{j}_1 + \mathbf{j}_2$  (Appendix D). The relative separation vector  $\mathbf{R}$  along the line of centers of mass of the two fragments lies in the body-fixed xy plane and is oriented at an angle  $\alpha_l$  with respect to the x axis  $(\alpha_l$  is conjugate to l). The vector  $\mathbf{R}$  and  $\alpha_l$  are not shown in Fig. 4(a), but are as depicted in Fig. 2, but with  $\mathbf{l} \times \mathbf{j}$  then replaced by  $\mathbf{l} \times \mathbf{k}$ .

Two coordinate frames  $(x_i', y_i', z_i')$  and  $(x_i'', y_i'', z_i'')$ , fixed in fragment  $X_i$  are defined. The doubly primed system is chosen so that the inertial tensor is diagonal in it; the  $z_i''$  axis is the symmetry axis of  $X_i$  if the latter happens to be a symmetric top. The primed system is chosen so that the  $z_i'$  axis lies along  $\mathbf{j}_i$ , and the  $x_i'$  axis lies along the intersection of  $x_i'$   $y_i'$  and  $x_i''$   $y_i''$  planes, namely along  $N_i'''$  in Fig. 4(a). The projections of  $\mathbf{j}_i$  on the z and  $z_i''$  axes are denoted by  $j_{iz}$  and  $\kappa_i$ , respectively [Fig. 4(a)].

The angles conjugate to  $(j_i, j_{iz}, \kappa_i)$  are, respectively,  $(\alpha_i, \beta_i, \gamma_i)$  as in Fig. 4(a). The z projection of l,  $l_z$ , its conjugate angle  $\beta_l$ , and  $\alpha_l$  specify the orientation of the body-fixed (x, y, z) system with respect to a space-fixed system. These coordinates provide a set of variables  $(l, \alpha_l, l_z, \beta_l, j_1, \alpha_1, j_{1z}, \beta_l, \kappa_1, \gamma_1, j_2, \alpha_2, j_{2z}, \beta_2, \kappa_2, \gamma_2)$  which specify, among other things, the orientation in space of each fragment  $X_i$  (i = 1, 2). Instead of  $(l_z, j_{1z}, j_{2z}, \beta_l, \beta_1, \beta_2)$  the variables  $(J, J_z, k, \alpha, \beta, \alpha_k)$  are used, where the symbols have the same meaning as in Appendix D. The resulting action variables are J,  $J_z$ ,  $J_1$ ,  $J_2$ , k, l,  $\kappa_1$ ,  $\kappa_2$  and their respective conjugate angles are  $\alpha$ ,  $\beta$ ,  $\alpha_1$ ,  $\alpha_2$ ,  $\alpha_k$ ,  $\alpha_l$ ,  $\gamma_1$ ,  $\gamma_2$ . Such action variables have been used previous

ly for symmetric tops in statistical phase space theory calculations of rotational sums and densities of states.<sup>45</sup>

#### 2. Density of transitional states

The expression for  $\Omega_J(\epsilon)$  is

 $\times \Delta (J, k, l) \Delta (k, j_1, j_2) \delta(\epsilon - H_{cl}).$ 

$$\Omega_{J}(\epsilon) = (2\pi)^{-8}\sigma^{-1} \int \cdots \int \times dJ_{z} \, dj_{1} \, dj_{2} \, dk \, dl \, d\kappa_{1} \, d\kappa_{2} \, d\alpha \, d\beta \, d\alpha_{1} \, d\alpha_{2} \, d\alpha_{k} \, d\alpha_{l} \, d\gamma_{1} \, d\gamma_{2}$$

The limits on the angle variables are 0 to  $2\pi$ , the  $J_z$  integral is over the interval (-J, J), the  $\kappa_i$  integrals are restricted by  $|\kappa_i| \leq j_i$ , and the angular momenta  $j_1, j_2$ , and l are restricted by the indicated triangle inequalities and by energy conservation. For  $X_1 \cdots X_2$  the Hamiltonian  $H_{cl}$  is written as

$$H_{\rm cl} = E_{r1} + E_{r2} + \frac{l^2}{2\mu R^2} + V_t(r_{mn}, \theta_1, \theta_2),$$
 (E2)

where  $\mu$  is the reduced mass for relative motion of the  $X_1$  and  $X_2$  fragments,  $r_{mn}$  (m,n=1-4) denotes a  $4\times4$  set of distances which, together with  $\theta_1$  and  $\theta_2$  are described in (3). When the  $X_i$ 's are symmetric tops, each rotational energy  $E_{ri}$  of a fragment  $X_i$  has the simple form  $J_i^2/2I_A + \kappa_i^2/2I_r$ . (The case of asymmetric tops is described at the end of this Appendix). The principal moments of inertia  $(I_A, I_B, I_C)$  of a fragment are determined from its R-dependent equilibrium geometry (Appendix C). In the particular case of CH<sub>3</sub> fragments  $I_A = I_B < I_C$ , each CH<sub>3</sub> is an oblate symmetrical top with symmetry axis C and with  $I_r = I_A I_C / (I_A - I_C) < 0$ . However, Eq. (E2) and the subsequent development apply to asymmetric tops as well, with a different expression for the rotational energy  $E_{ri}$ . The relation between the action-angle variables and the internal coordinates for the particular case of the  $C_2H_6 \rightarrow CH_3 \cdot \cdot \cdot CH_3$  system is described in Sec. 3.

#### 3. Internal coordinates

For a system such as  $C_2H_6\rightarrow 2$  CH<sub>3</sub> the potential  $V_t$  is modeled to be a function of the  $r_{mn}$  (m,n=1,2,3,4), which are the separation distances between atoms (four per fragment) of the two fragments, and a function of the angle  $\theta_i$  between the C-C axis and the symmetry axis  $z_i''$  of fragment i (i=1,2). Some of these coordinates are identified in Fig. 4(b). The coordinates  $r_{\rm CH}$  and  $\alpha_{\rm HCH}$  which determine the CH<sub>3</sub> structure are implicitly included in the state counting in  $N_V(E'-\epsilon)$ . The reaction coordinate R, the angular momenta  $j_1, j_2, l$ , and the projections  $\kappa_1, \kappa_2$  are depicted in Fig. 4(c) for this system.

The CH<sub>3</sub> structure determines the atomic position vectors  $\mathbf{r}_n^{(i)}$  in the fragment-fixed  $(x_i'', y_i'', z_i'')$  system. The vectors  $\mathbf{r}_n^{(i)}$  are then obtained from  $\mathbf{r}_n^{(i)'}$  by two successive applications of the inverse rotation matrix  $\mathbf{A}^{-1}$ <sup>29</sup>:

$$\mathbf{r}_n^{(i)} = \mathbf{A}^{-1}(\alpha_i, \, \theta_{li}, \, \boldsymbol{\beta}_i) \mathbf{A}^{-1}(\gamma_i, \, \theta_{\kappa,i}, 0) \mathbf{r}_n^{(i)^*}. \tag{E3}$$

Here,  $\beta_i$  is the angle from the x axis to the line of nodes  $N_i'$  in Fig. 4(a) (the intersection of the xy and  $x_i'$   $y_i'$  planes),  $\theta_{li}$  is the angle between the z and  $z_i'$  axes and  $\alpha_i$  is the angle from  $N_i'$  to the  $x_i'$  axis. Again, the zero in Eq. (E3) indicates that the angle from the  $x_i'$  axis to the line of nodes  $N_i'''$  (the intersec-

tion of  $x_i'$   $y_i'$  and  $x_i''$   $y_i''$  planes) is zero,  $\theta_{\kappa_i}$  is the angle between the  $z_i'$  and  $z_i''$  axes, and  $\gamma_i$  is the angle from  $N_i'''$  to the  $x_i''$  axis. Some of these various angles are described in Fig. 4(a). The separation vector  $\mathbf{R}$  is given by

$$\mathbf{R} = \mathbf{A}^{-1}(\alpha_1, 0, 0)\mathbf{R}^*,\tag{E4}$$

where  $\mathbb{R}^*$  is a column vector with components (R,0,0).

To express  $V_t$ , and hence  $H_{\rm cl}$  in Eq. (E2) in terms of J, R,  $r_{\rm CH}$ ,  $\alpha_{\rm HCH}$ , and the integration variables in Eq. (E2), one needs to express  $\theta_1$ ,  $\theta_2$ , and the  $r_{mn}$ 's in terms of those variables. The coordinates  $(R, \alpha_l, r_{\rm CH}, \alpha_{\rm HCH}, \alpha_i, \theta_{li}, \beta_i, \gamma_i, \theta_{\kappa_i})$  specify, in the body-fixed (x, y, z) system, the following quantities:  $\mathbf{R}$ , the orientation  $\mathbf{e}_{z_i^n}$  of the symmetry axis of  $X_i$  and the position vectors  $\mathbf{r}_n^{(l)}$  of the four atoms (n=1,2,3,4) in  $(\mathrm{CH}_3)_i$  with respect to the center of mass of  $(\mathrm{CH}_3)_i$  (i=1,2). From the above quantities, the internal coordinates  $\cos\theta_i=\mathbf{e}_{r_{cc}}\cdot\mathbf{e}_{z_i^n}(i=1,2)$  and  $r_{mn}=|\mathbf{R}+\mathbf{r}_m^{(1)}-\mathbf{r}_n^{(2)}|$   $(m,n=1,\ldots 4)$  are readily determined. R is fixed beforehand,  $\alpha_l$  is a variable of integration, and  $r_{\rm CH}$  and  $\alpha_{\rm HCH}$  are each set equal to their R-dependent equilibrium values  $r_{\rm CH,e}$  and  $\alpha_{\rm HCH,e}$  (Appendix C).

The angles  $\alpha_i$ ,  $\alpha_i$ , and  $\gamma_i$  in Eqs. (E3) and (E4) are defined in Table I;  $\theta_{\kappa_i} = \cos^{-1}(\kappa_i/j_i)$ ;  $\theta_{li}$  is defined in Table II;  $\beta_i$ , the angle between  $l \times k$  [which lies along the x axis in Fig. 4(a)] and  $N_i' = (l \times j_i)$ , is specified in the interval  $(0, 2\pi)$  by Eqs. (E5) and (E6):

$$\cos \beta_i = [\cos \theta_{ki} - \cos \theta_{li} \cos \theta_{lk}] / [\sin \theta_{li} \sin \theta_{lk}].$$
(E5)

Equation (E5) follows from Eq. (7) with **a**, **b**, **c**, **d** identified as in Table III. To determine the quadrant for  $\beta_i$  one can use a vector identity<sup>46</sup> and ultimately obtain

$$\sin \beta_i = \mp \sin \theta_{ki} \sin \alpha_k / \sin \theta_{li}, \tag{E6}$$

where the minus sign is for i = 1 and the plus sign for i = 2. The sign difference arises from the fact that  $\mathbf{j}_1 \times \mathbf{k} = -\mathbf{j}_2 \times \mathbf{k}$ . The conjugate angle  $\alpha_k$  in Eq. (E6) is defined in Table I; the angles  $\theta_{ki}$  and  $\theta_{lk}$  in Eqs. (E5) and (E6) are defined in Table II.

 $H_{\rm cl}$  is specified by the variables  $(R, r_{\rm CH}, \alpha_{\rm HCH}, J, l, k, j_1, j_2, \kappa_1, \kappa_2, \alpha_k, \alpha_l, \alpha_1, \alpha_2, \gamma_1, \gamma_2)$  and is independent of  $(J_z, \alpha, \beta)$ . Equation (E1) now becomes

$$\Omega_{J}(\epsilon) = (2J+1)(2\pi)^{-6}\sigma^{-1}\int \cdots \int \\
\times dj_{1} dj_{2} dk dl d\kappa_{1} d\kappa_{2} d\alpha_{1} d\alpha_{2} d\alpha_{k} d\alpha_{l} d\gamma_{1} d\gamma_{2} \\
\times \Delta (J,k,l)\Delta (k,j_{1},j_{2})\delta(\epsilon - H_{cl})$$
(E7)

and

$$N_{EJ} = (2J+1)(2\pi)^{-6}\sigma^{-1}\int\cdots\int$$

$$\times dj_1 dj_2 dl dk d\kappa_1 d\kappa_2 d\alpha_1 d\alpha_2 d\alpha_k d\alpha_1 d\gamma_1 d\gamma_2$$

$$\times N_V(E'-H_{cl})\Delta (J,k,l)\Delta (k,j_1,j_2). \tag{E8}$$

The evaluation of Eq. (E8) is described in Sec. III.

#### 4. Asymmetric top case

We conclude this Appendix with a discussion of the asymmetric top case, to replace the expression given for  $E_n$ 

following Eq. (E2).

In the fragment-fixed  $(x_i'', y_i'', z_i'')$  frame in which the projection of  $\mathbf{j}_i$  on the  $z_i''$  axis is  $\kappa_i = j_{iz''}$  and in which the inertia tensor is diagonal, the rotational energy of a rigid asymmetric top with principal moments  $I_A \neq I_B \neq I_C$  is

$$E_{ri} = (j_{ix''}^2/2I_A) + (j_{iy''}^2/2I_B) + (j_{iz''}^2/2I_C).$$
 (E9)

Unlike  $\kappa_i$ ,  $j_{ix}$  and  $j_{iy}$  are not variables of integration in Eqs. (E7) and (E8) but are readily specified in terms of these variables by rotating the coordinate axes from the primed to the doubly primed system, i.e.,

$$\mathbf{j}_{i}^{"} = \mathbf{A}(\gamma_{i}, \theta_{\kappa i}, 0)\mathbf{j}_{i}^{'}, \tag{E10}$$

where  $\mathbf{j}_{i}''$  and  $\mathbf{j}_{i}'$  are column vectors with components  $(j_{ix''}, j_{ix''})$  and  $(0,0,j_{i})$ , respectively. Equation (E10) yields  $j_{ix}'' = j_{i} \sin \theta_{\kappa_{i}} \sin \gamma_{i}, \ j_{iy}'' = j_{i} \sin \theta_{\kappa_{i}} \cos \gamma_{i}, \ j_{iz}'' = j_{i} \cos \theta_{\kappa_{i}}. \tag{E11}$ 

We turn next to the value of the  $\sigma$  in Eq. (E8). When the CH<sub>2</sub>'s are planar, as they are in a loose transition state, the value of  $\sigma$  is  $6 \times 6 \times 2 = 72$ . When the transition state is more restricted, as at smaller R<sup>†</sup>'s, each CH<sub>3</sub> lies in a double-well potential for the out-of-plane H<sub>3</sub> vs C motion, and the stablest CH<sub>3</sub> configuration is now bent. For the case that the transition state is still nearly loose, we shall freeze each CH<sub>3</sub> in a bent configuration, count the phase space as before, and use  $\sigma = 72$ , thus ensuring that the phase space divided by  $\sigma$  is a continuous function of R at large R's. If the transition state were instead quite tight, one of the two wells of this doublewell potential would disappear, and  $\sigma$  would equal 18, in the case of free internal rotation about the CC axis. An interpolation formula between these two limiting situations can be designed, or a more elaborate treatment for the out-of-plane CH, motion can be given. (For example, these two coordinates can be included in the transitional modes, and either treated classically or current path integral techniques can be used in the Monte Carlo calculations to treat them quantum mechanically, in the presence of the remaining classical-like transitional modes.) However, these refinements are omitted in the present paper.

#### APPENDIX F: MONTE CARLO CALCULATION OF $N_{E,I}$

1. N<sub>EJ</sub>

The Monte Carlo evaluation of  $N_{EJ}$  is described in this Appendix using the reaction  $C_2H_6\rightarrow 2CH_3$  as an illustration. The calculations for  $NO_2\rightarrow NO+O$  and  $H_2O_2\rightarrow 2OH$  were analogous. To evaluate the 12-dimensional integral appearing in Eq. (E8), a 12-dimensional vector  $\xi$  is first defined whose components  $\xi_k$  are random numbers uniformly distributed on the interval (0, 1). In obtaining a particular  $\xi$  an additional random number was used to shuffle 13 the order in which the 12 numbers were obtained from a pseudorandom number generator, to avoid the possible repetitive assignment of correlated n-tuples to the same  $\xi_i$ 's. The assignment of the action-angle variables in Eq. (E8) to the  $\xi_i$ 's were as follows:

$$j_i = \xi_i j_i^{\text{max}} \ (i = 1, 2),$$

$$\begin{split} k &= k^{\min} + (k^{\max} - k^{\min})\xi_3, \\ l &= l^{\min} + (l^{\max} - l^{\min})\xi_4, \\ \kappa_i &= 2j_i(\xi_{i+4} - 1/2), \alpha_i = 2\pi\xi_{i+6}, \gamma_i = 2\pi\xi_{i+8} \ (i = 1, 2), \\ \alpha_k &= 2\pi\xi_{11}, \ \alpha_l = 2\pi\xi_{12}, \end{split}$$

where  $j_{l}^{\max}$  equals  $[2I_{C}(R)E_{rl}^{\max}]^{1/2}$  for an oblate top  $(I_{C}>I_{A}=I_{B})$ , with  $E_{r1}^{\max}=E'$  and  $E_{r2}^{\max}=E'-E_{r1}(j_{1},\kappa_{1})$ ;  $k^{\min}$  is  $|j_{1}-j_{2}|$ ,  $k^{\max}$  is  $j_{1}+j_{2}$ ,  $l^{\min}$  is |J-k|,  $l^{\max}$  is  $\min[J+k, (2\mu R^{2}E_{l}^{\max})^{1/2}]$ , and  $E_{l}^{\max}$  is  $(E'-E_{r1}-E_{r2})$ .

Introducing the transformation equation (F1) into Eq. (E8) yields

$$N_{EJ} = (2J+1) \int \cdots \int d\xi \ G(\xi), \tag{F2}$$

with  $d\xi$  denoting  $d\xi_1 \cdots d\xi_{12}$  and

$$\begin{split} G(\xi) &= j \frac{\max}{1} j \frac{\max}{2} (k^{\max} - k^{\min}) \\ &\times (l^{\max} - l^{\min}) 2 j_1 2 j_2 N_{\nu} (E' - H_{\text{cl}}) \\ &\times \theta (k^{\max} - k^{\min}) \theta (l^{\max} - l^{\min}) \\ &\times \theta (|\kappa_1| - \kappa_1^{\min}) \theta (|\kappa_2| - \kappa_2^{\min}). \end{split} \tag{F3}$$

The step functions  $\theta$  for  $\kappa_1$  and  $\kappa_2$  are an additional restriction arising from the requirement that  $E_{ri}$  be nonnegative. For an oblate symmetric top and for a given  $j_i$ , this condition leads to  $\kappa_i^{\min}$  being equal to  $\{-2I_r(R)[E_{ri}^{\max}-j_i^2/2I_A(R)]\}^{1/2}$  if  $j_i$  is greater than  $j_i^{\min}=[2I_A(R)E_{ri}^{\max}]^{1/2}$  and equal to 0 otherwise. (As noted in Appendix E,  $I_r$  is negative.) For other types of tops different restrictions apply. A Monte Carlo estimate for  $N_{EJ}$  in terms of  $G(\xi)$  is

$$N_{EJ}^{MC} = (2J+1)\sum_{n=1}^{N} G(\xi_n)/N$$

with

$$\sigma^{\text{MC}} = \left\{ |(N_{EJ}^{\text{MC}})^2 - (2J+1)^2 \sum_{n=1}^{N} [G(\xi_n)]^2 / N |/N| \right\}^{1/2},$$
(F4)

where N is the number of Monte Carlo points. Accumulated intermediate results for  $N_{EJ}^{MC}$  and  $\sigma^{MC}$  were examined at equally spaced increments of  $\Delta n = N/10$  and provided a useful assessment of the convergence for a given N.

#### 2. Variance reduction

When the number of rejected points in Eq. (F4), i.e., the number of terms with  $G(\xi_n) = 0$  is reduced for a given N, the convergence of  $N_{EJ}^{MC}$  is improved. As a first step it was found that choosing  $j_1$  and  $j_2$  as the outer variables of integration in Eq. (E8), instead of l for example, significantly reduced  $\sigma^{MC}$ . The technique of uniform stratification l was next applied to the outer integration variable  $j_1$ . For subintervals of length  $\Delta j_{1,k} = f_1^{\max}/5(k=1,2,...5)$  it was found that only a variance reduction of  $\sim 10\%$  occurred when equal numbers of points  $N_k = N/5$  were used in each subinterval, as compared to no stratification using the same number of integration points. More importantly, however, this procedure revealed orders-of-magnitude differences between contributions  $N_{EJ,k}^{MC}$  to  $N_{EJ}^{MC}$  from some of the five subintervals. Those subintervals

with larger contributions were also found to have larger variances, making it clear that increasing the sampling of these bins relative to those with smaller contributions would decrease the overall variance for a given N.

In importance sampling, we recall, some weighting function is used for the sampling. In the case of the present integral with its complicated limits a weighting function for the integration variables was not immediately obvious. Instead, an empirical weighting function in histogram form was obtained for  $j_1$  by preliminary uniform sampling, as above, and then that histogram was used in the importance sampling. <sup>13</sup>

To obtain an appropriate nonuniform random number distribution for  $j_1$  the uniform stratification described above was used to provide approximate values of  $N_{EJ,m}^{MC}$ . This procedure typically utilized  $3\Delta n$  or  $4\Delta n$  points of the total of  $N(=10\Delta n)$  points. A cumulative distribution vector<sup>13</sup>  $\{C_1, C_2,...\}$  for the bin values was obtained in histogram form:

$$C_k = \sum_{m=1}^{k} N_{EJ,m}^{\text{MC}} / \sum_{m=1}^{5} N_{EJ,m}^{\text{MC}} \quad (k = 1-5).$$
 (F5)

The remaining  $N-4\Delta n$  or  $N-3\Delta n$  Monte Carlo integration points were chosen as follows: Together with each 12-component random number, an additional random number  $\xi_{13}$  uniformly distributed on (0, 1) was generated. The bin k of width  $\Delta j_{1,k}$  to which  $j_1$  was assigned was determined as the k for which  $C_k > \xi_{13} > C_{k-1}$ . The  $j_1$  value was then chosen uniformly within this k th bin according to the random variable  $\xi_1$ ; all other variables were selected in the manner described previously [cf. Eq. (F1)]. The next choice of  $\xi_1, \dots, \xi_{13}$  was then made and the entire procedure repeated until the remaining  $N-4\Delta n$  or  $N-3\Delta n$  points were used.

#### 3. $N_{\nu}$

For NO<sub>2</sub> $\rightarrow$ NO + O,  $N_V$  was determined explicitly for each Monte Carlo point  $\xi_n$ . For the Morse oscillator model of the NO vibration, the classical vibrational energy  $E'_V$  in excess of the zero point energy in units of  $\hbar = 1$  is  $(4D/k^2)[(x+\frac{1}{2})k-(x+\frac{1}{2})^2-(\frac{1}{2})k+(\frac{1}{2})^2]$ , where k is a dimensionless quantity (in units of  $\hbar = 1$ )  $2\sqrt{2\mu D}/\beta$ ,  $\mu$  is the NO reduced mass, the Morse parameters D and  $\beta$  are those in Appendix A, and  $2\pi(x+\frac{1}{2})$  is the classical vibrational action, <sup>11</sup> x being a continuous variable, the classical equivalent of a "quantum number." This equation for  $E'_V(x)$  is readily inverted to yield  $x(E'_V)$ . With  $E'_V$  equal  $E'-H_{cl}(\xi_n)$ , the corresponding maximum vibrational quantum number  $n^{\max}$  is the greatest integer less than or equal to x and the number of vibrational states with energy  $E'_V \leq E' - H_{cl}(\xi_n)$  is  $N_V = n^{\max} + 1$ .

For  $H_2O_2 \rightarrow 2$  OH,  $N_V$  was also determined explicitly for each Monte Carlo point  $\xi_n$  via the Morse oscillator model of the two OH vibrations (Appendix B). The vibrational quantum numbers of the OH bonds are the integers  $n_1$  and  $n_2$ . The value of  $n_2$  goes from zero to a maximum  $n_2^{\max}$ , obtained as the greatest integer for which  $E'_{V2}$ , the vibrational energy of this second bond in excess of its zero point energy,  $\leqslant E' - H_{cl}(\xi_n) - E'_{V1}(n_1)$ . That is,  $n_2^{\max}$  is a function of  $n_1$ . The maximum value of  $n_1$ ,  $n_1^{\max}$ , is the greatest integer for

which  $E'_{V1} \leq E' - H_{cl}(\xi_n)$ . The total number of vibrational states  $N_V$  is the sum

$$\sum_{n_1=0}^{n_1^{\max}} [n_2^{\max}(n_1)+1].$$

For C<sub>2</sub>H<sub>6</sub>→2 CH<sub>3</sub>, the greater number of vibrational modes and the increased dimensionality of the  $N_{EJ}$  integral make a specific evaluation of  $N_V$  for each Monte Carlo point undesirable.  $N_{\nu}$  was determined as a function of  $E'_{\nu}$  before evaluating Eq. (E8) as follows. For the purpose of counting the vibrational states of the two identical CH<sub>3</sub> fragments there are, in total, two doubly degenerate modes with frequencies  $v_1$  and  $v_2$ , and two quadruply degenerate modes with frequencies  $v_3$  and  $v_4$ . These frequencies are assumed to depend on R as in Eq. (C2). Denoting the principal quantum numbers for these four modes by  $n_i$  (i = 1-4) one can write the total vibrational energy E'<sub>V</sub> in excess of the zero point energy as  $2\pi(n_1v_1 + n_2v_2 + n_3v_3 + n_4v_4)$  in units of  $\tilde{n} = 1$ . The corresponding degeneracy w is  $w_{n_1}^{(2)} w_{n_2}^{(2)} w_{n_3}^{(4)} w_{n_4}^{(4)}$ , where  $w_{n_i}^{(d_i)}$  equals  $(n_i + d_i - 1)!/n_i!(d_i - 1)!$  and  $d_i$  is the degeneracy of the *i*th oscillator.<sup>47</sup> All quartets  $(n_1, n_2, n_3, n_4)$  were determined such that  $E'_{\nu} \leq E'$  and the corresponding degeneracy w was assigned to a linear array based on an energy grid of  $\Delta E = 1 \text{ cm}^{-1}$  (although in practice 10 cm<sup>-1</sup> would undoubtedly have sufficed). The number of vibrational states  $N_{\nu}(E'_{n})$  with energy less than or equal to  $E'_{n}$   $(=n\Delta E)$  is given by the sum  $\sum_{k=1}^{n} g_k$ , where k is an array index:  $g_k = 0$ if there is no vibrational state in the kth  $E'_{V}$  interval  $[(k-1)\Delta E, k\Delta E]$ , and  $g_k$  is the value of the sum of the degeneracies w for states in that interval  $(g_1 = 1)$  for the ground state). For each Monte Carlo point  $\xi_n$ ,  $N_{\nu}(E'_n)$  was simply read from the array with index determined from the value of  $E'_n[=E'-H_{cl}(\xi_n)]$ . The grid size chosen is a compromise between computer memory requirement and the inaccuracy associated with multiple entries in the same array position (a very minor inaccuracy for a small grid size). Multiple entries appeared only at higher energies where vibrational levels are closely spaced. Analysis of the computational results for  $C_2H_6\rightarrow 2$  CH<sub>3</sub> indicated that at low values of  $\epsilon[=H_{cl}(\xi_n)]$ and hence at high  $E'_{\nu}$  (=  $E' - \epsilon$ ) values, there was little contribution of multiple entries to  $N_{EJ}^{MC}$  for the (E, J) values used in the present study. For the largest E' (and hence  $E'_{\nu}$ ) used,  $\sim 122 \text{ kcal mol}^{-1}$ , approximately 4% of the array positions had multiple entries.

#### APPENDIX G: VARIABLE REDUCTION FOR $J=\mathbf{0}$ CASE

(a)  $NO_2 \rightarrow NO + O$ : If J = 0, then j = l = 0, j = l, and  $\cos \theta_{lj} = -1$ . That is the  $\Delta$  in Eq. (8) becomes  $\delta(j - l)$ . Equation (6) becomes

$$\cos \gamma = \cos(\alpha_1 + \alpha_j). \tag{G1}$$

The integrand is now independent of  $\alpha_l - \alpha_j$ . Writing  $\theta_s = \frac{1}{2}(\alpha_l + \alpha_j) = \frac{1}{2}\gamma$ ,  $\theta\omega_d = \alpha_l - \alpha_j$ , and introducing the function  $\delta(j-l)$  in Eq. (8), a two-dimensional integral is obtained. After integrating over the appropriate  $(\theta_s, \theta_d)$  domain<sup>48</sup> one obtains

$$\Omega_{J=0}(\epsilon) = (2\pi)^{-2} \int dj \int dl \int d\theta_s \int d\theta_d \, \, \delta(j-l) \delta(\epsilon - H_{\rm cl})$$

$$= 2(2\pi)^{-1} \int dj \int_0^{\pi} d\theta_s \, \, \delta(\epsilon - H_{\rm cl}). \tag{G2}$$

The same property, namely that the integrand is independent of an angle  $\theta_d$ , will be true in (b) and (c) also.

(b)  $H_2O_2 \rightarrow 2OH$ : if J = 0, then l + k = 0, k = l,  $\cos \theta_{lk} = -1$ , and  $\cos \theta_{li} = -\cos \theta_{ki}$  (i = 1, 2). The reference axis x for the angles of  $\alpha_l$  and  $\alpha_k$  (see Table I) is no longer defined since  $l \times k = 0$ . Equation (D6) becomes

$$\cos \theta_R = \cos(\alpha_k + \alpha_l). \tag{G3}$$

We redefine  $\theta_R = \alpha_k + \alpha_l$  as the angle between  $\mathbf{j}_1 \times \mathbf{j}_2$  and  $\mathbf{R}$  and  $\theta_{ri} = \alpha_i$  as the angle between  $\mathbf{j}_1 \times \mathbf{j}_2$  and  $\mathbf{r}_i$ .

Equation (7) with  $(\mathbf{a}, \mathbf{b}, \mathbf{c}, \mathbf{d}) = (\mathbf{j}_1 \times \mathbf{j}_2, \mathbf{r}_i, \mathbf{j}_1 \times \mathbf{j}_2, \mathbf{R})$  yields

$$\cos \gamma_i = \cos \theta_R \cos \alpha_i + \sin \theta_R \sin \alpha_i \cos \theta_{li}. \tag{G4}$$

Introducing the variables  $\theta_s = \frac{1}{2}(\alpha_l + \alpha_k) = \frac{1}{2}\theta_R$  and  $\theta_d = \alpha_l - \alpha_k$  and, for  $\Delta$ , the function  $\delta(l - k)$  in Eq. (D8) one obtains the six-dimensional integral

$$\Omega_{J=0}(\epsilon)=2(2\pi)^{-3}\int\cdots\int$$

 $\times dj_1 dj_2 dk d\alpha_1 d\alpha_2 d\theta_s \Delta(k, j_1, j_2) \delta(\epsilon - H_{cl}),$  (G5)

where  $\alpha_1$  and  $\alpha_2$  vary from 0 to  $2\pi$  and  $\theta_s$  varies from 0 to  $\pi$ . (c)  $C_2H_6\rightarrow 2CH_3$ : As for  $H_2O_2\rightarrow 2OH$  k=l,  $\cos \theta_{lk} = -1$ ,  $\cos \theta_{li} = -\cos \theta_{ki}$  (i = 1, 2), and the reference axis  $l \times k$  for  $\alpha_l$  and  $\alpha_k$  (see Table I) is again no longer defined. In addition the Euler angle  $\beta_i$  between  $1 \times k$  and  $1 \times j$ , needs to be redefined. In the special case of J = 0,  $1 \times j_1 = j_1 \times k = j_1 \times j_2$  $1 \times \mathbf{j}_2 = \mathbf{j}_1 \times \mathbf{k} = \mathbf{j}_2 \times \mathbf{j}_1$ . From the definition of  $\alpha_k$  in Table I, it is seen that  $\alpha_k$  and  $\beta_1$  now define rotations between the same axes in the xy plane. The sense of these rotations is opposite since  $\beta_1$  is a rotation about the z axis which lies along I and  $\alpha_k$  is a rotation about k which lies along -1. This is verified by simplifying Eqs. (E5) and (E6) using  $\cos \theta_{lk} = -1$ ,  $\sin \theta_{lk} = 0$ , and  $\cos \theta_{ki} = -\cos \theta_{li}$ , giving  $\cos \beta_1 = \cos \alpha_k$  and  $\sin \beta_1 = -\sin \alpha_k$ , or  $\beta_1 = -\alpha_k$ . Similarly, it can be shown that  $\beta_2 = \pi - \alpha_k$ . The integrand depends on the angle between **R** and  $\mathbf{j}_1 \times \mathbf{j}_2$ , namely,  $\beta'_1$  $= |\beta_1 - \alpha_l| = |-\alpha_k - \alpha_l| = \alpha_l + \alpha_k.$ therefore, the variables  $\theta_s = \frac{1}{2}(\alpha_l + \alpha_k)$  and  $\theta_d = \alpha_l - \alpha_k$ and the function  $\delta(l-k)$  in Eq. (E7) yields the ten-dimensional integral

$$\Omega_{J=0}(\epsilon) = 2(2\pi)^{-5} \int \cdots \int \\ \times dj_1 \, dj_2 \, dk \, d\kappa_1 \, d\kappa_2 \, d\alpha_1 \, d\alpha_2 \, d\theta_s \, d\gamma_1 \, d\gamma_2 \\ \times \Delta \, (k, j_1, j_2) \delta(\epsilon - H_{cl}), \tag{G6}$$

where  $\beta_1'(=2\theta_s)$  and  $\beta_2'(=\pi+\beta_1')$  replace  $\beta_1$  and  $\beta_2$  in Eq. (E3) and where the x axis is now taken to lie along **R**.

## APPENDIX H: SOME RELEVANT NOTES ON THE PRESENT CALCULATIONS WITH SACM METHOD

The SACM method uses, as in RRKM theory, Eq. (1), but differs in the method for counting  $N_{EJ}$ . It is assumed that vibrationally adiabatic eigenvalues  $E_a(q)$  can be found for

any value of the reaction coordinate q by interpolating between reactant  $(q=q_e)$  and product  $(q=\infty)$  eigenvalues by a universal exponential interpolation function g(q). Specifically, it is assumed that

$$\begin{split} E_a(q) &= E_a(n_p, \infty) \\ &+ \left[ E_a(n_p, g_e) - E_a(n_p, \infty) \right] g(q) + E_{\text{cent}}(q) + V(q), \end{split}$$
 (H1)

where V(q) is the potential along q, and  $n_p$  and  $n_r$  denote the totality of quantum numbers for motion transverse to q for products and reactants respectively;  $E_{\rm cent}$  is a centrifugal term, assumed to be  $P(P+1)/2\bar{I}(q)$ , with P equal to l+(J-l)g(q), l is the orbital angular momentum of the fragments, restricted to lie between |J-j| and J+j, and  $\bar{I}$  is the mean of the two larger principal moments of inertia of ONO for a fixed bending angle. The interpolation function g(q) and the Morse potential for V(q) are given in Appendix A with q identified as the ONO separation distance.

The reactant-product correlation in Eq. (H1) is subject to conservation of J and to vibrational adiabaticity for those modes whose quantum numbers are assumed to be conserved. In practice, product vibrations were correlated on a 1:1 basis with appropriate reactant vibrations. Only "adiabatic channels" whose eigenvalue maxima are less than the final asymptotic available energy are, or course, counted in  $N_{EJ}$ . Either symmetry-adapted counts can be made (i.e., correlating only states of the same symmetry) or all states can be counted and then corrected by introduction of approximate symmetry-correction factors. <sup>19</sup> In comparing the present method with SACM calculated results only total numbers of states were utilized and no symmetry corrections were introduced.

For the particular case of  $NO_2 \rightarrow NO + O$ ,  $E_a(n_p, \infty)$  was written (in units of  $\hbar = 1$ ) as

$$E_a(n_p, \infty) = (4D_{NO}/k_{NO}^2) \left[ (v + \frac{1}{2})k_{NO} - (v + \frac{1}{2})^2 \right] + \left[ j(j+1)/2\mu_{NO} r_e^2 \right],$$
 (H2)

where  $n_p$  denotes the pair (v, j),  $\mu_{NO}$  is the reduced mass of NO,  $r_e$  is the equilibrium NO bond length, and  $k_{NO}$  equals  $2(2\mu_{NO}D_{NO})^{1/2}/\beta_{NO}$  in units of  $\hbar=1$ .  $E_a(n_r,q_e)$  was written as

$$\begin{split} E_a(n_r, q_e) &= (4D_{\text{ON-O}}/k_{\text{NO-O}}^2) \left[ (v + \frac{1}{2}) k_{\text{ON-O}} - (v + \frac{1}{2})^2 \right] \\ &+ (v_b + \frac{1}{2}) \hbar v_2 + (\kappa^2 / 2I_{re}), \end{split} \tag{H3}$$

where  $n_r$  denotes  $(v, v_b, \kappa)$ ;  $v_2$  is the ONO bending frequency and the last term in Eq. (H3) denotes an "internal" rotational energy contribution to a prolate symmetric top model for NO<sub>2</sub> the restriction  $|\kappa| \leq J$  is used.  $I_{re}$  equals  $I_{Ae}\bar{I}_e/(\bar{I}_e-I_{Ae})$ , where  $\bar{I}_e$  is the arithmetic mean of  $I_{Be}$  and  $I_{Ce}$ . The three principal moments of inertia of NO<sub>2</sub> are listed in Table A1, together with other properties.

#### APPENDIX I: $F_{\rho}(E'_r, J)$

An approximate correction factor  $F_{\rho}(E',J)$  for rotation about the symmetry axis is readily obtained. For a symmetric top molecule with angular momentum projection K along the symmetry axis the rovibrational state density is

$$\rho_{vr}(E', J) = (2J+1) \int_{-K_{max}}^{K_{max}} \rho_{v} \left[ E', -E_{rot}(J, K) \right] dK,$$
(I)

where  $E'_r$  is the total energy available to the reactant in excess of the zero point energy, the sum over K was replaced by the integral, and  $K_{\max}$  is given below. For a prolate top such as ethane with  $I_{A,r} = I_{B,r} > I_{C,r} E_{\text{rot}}$  equals  $J^2/2I_{A,r} + K^2/2I_{r,r}$  (in units of  $\hbar = 1$ ), where  $I_{r,r} = I_{A,r}I_{C,r}/(I_{A,r} - I_{C,r})$  and  $K_{\max} = \min \{J_r(2I_{r,r}x)^{1/2}\}$ , and  $X_r = I_{A,r}I_{C,r}/(I_{A,r}x)^{1/2}$  and  $X_r = I_{A,r}I_{C,r}/(I_{A,r}x)^{1/2}$  where  $I_{r,r} = I_{A,r}I_{C,r}/(I_{A,r}x)^{1/2}$  and  $I_{A,r}I_{C,r}/(I_{A,r}x)^{1/2}$  and  $I_{A,r}I_{C,r}/(I_$ 

$$\frac{\rho_{vr}(E',J)}{(2J+1)} = \frac{(x+aE_{Zr})^{s-1}}{\Gamma(s)\prod_{i=1}^{s}h\nu_{i}} \times \sqrt{2I_{r,r}(x+aE_{Zr})} \int_{0}^{y} dy \, y^{-1/2} (1-y)^{s-1} \\
\equiv \rho_{v}(x)F_{\rho}(x,J), \tag{I2}$$

where y equals  $(K_{\max}^2/2I_{r,r})/(x+aE_{Zr})$ .

When  $K_{\text{max}}$  is determined by an energy requirement, namely that  $K_{\text{max}}^2 = (2I_{r,r}x)^{1/2}$ , Y is close to unity. When, instead, J is very small,  $K_{\text{max}}$  equals J, Y is less than unity; typically only a little angular momentum was needed for the Y to be close enough to unity for the integral in Eq. (I2) to become the Beta function  $B(\frac{1}{2}, s)$ :

$$F_{\rho} \cong \sqrt{2I_{r,r}(x + aE_{Zr})}B\left(\frac{1}{2}, s\right). \tag{I3}$$

More generally, the integral in Eq. (I2) is  $Y^{1/2}$  time the hypergeometric function  $F(1-s,\frac{1}{2};\frac{3}{2};Y)^{49}$  and  $F_{\rho}$  can then be written as<sup>49</sup>

$$F_{\rho}(x,J) = \sqrt{2I_{r,r}(x + aE_{Zr})} 2Y^{1/2} \times \left\{ 1 + \sum_{i=1}^{s-1} Y^{i} \left[ \prod_{j=1}^{i} (j-s) \right] / (2i+1)i! \right\}.$$
 (I4)

For a given rotational energy E', one can define a  $J_{\rm max}$  as  $\{2I_{\rm A,e}E'_{\rm c}\}^{1/2}$  and a  $J_{\rm min}$  as  $\{2I_{\rm C,e}E'_{\rm c}\}^{1/2}$ . There are two cases to consider in evaluating the sum in Eq. (I4): (a)  $0 \le J \le J_{\rm min}$ : In this case  $K_{\rm max} = J$  and so  $Y = J^2/2I_{\rm r,r}(x + aE_{Zr})^{-1}$ , which is less then unity. (b)  $J_{\rm min} < J < J_{\rm max}$ : Here,  $K_{\rm max} = \{2I_{\rm r,r}x\}^{1/2}$ , which is less than J, and so  $Y = x/(x + aE_{Zr})$ . When x considerably exceeds  $aE_{Zr}$ ,  $Y \cong 1$  and Eq. (I3) is obtained, in agreement with a corresponding expression,  $^{26(a)}$  when  $B(\frac{1}{2}, s)$  is written in terms of gamma functions. Typical ratios of the value of  $F_{\rm A}$  to that given by Eq. (I4) where 0.65, 0.95, and 1 when J = 25, 50, and 75 or greater, depending on the energy. For example, at J = 25, the ratio was 0.68 and 0.58 at  $E'_{\infty} = 0.44$  and 63.5 kcalmof<sup>-1</sup>, respectively. Typically, for the  $C_2H_6 \rightarrow 2CH_3$  reaction at room temperature, the most probable of J is 25 and is higher at high temperatures.

The rotational factor  $F_{\rho}$  described above is for a microcanonical rate constant. Other rotational factors have been described for the thermal rate constant. <sup>26(b),50</sup>

M. Wardlaw and R. A. Marcus, Chem. Phys. Lett. 110, 230 (1984).
 R. A. Marcus, J. Chem. Phys. 20, 359 (1952); R. A. Marcus and O. K. Rice, J. Phys. Colloid Chem. 55, 894 (1951).

<sup>3</sup>See Ref. 1 and references cited therein.

<sup>4</sup>R. A. Marcus, J. Chem. Phys. 43, 2658 (1965); 52, 1018 (1970).

<sup>5</sup>E. Wigner, J. Chem. Phys. 5, 720 (1937); Trans. Faraday Soc. 34, 29 (1938); J. Horiuti, Bull Chem. Soc. Jpn. 13, 210 (1938); J. C. Keck, J. Chem. Phys. 32, 1035 (1960); Adv. Chem. Phys. 13, 85 (1967); D. G. Truhlar, W. L. Hase, and J. T. Hynes, J. Phys. Chem. 87, 2664 (1983), and references cited therein.

<sup>6</sup>See, for example, R. A. Marcus, J. Chem. Phys. 20, 359 (1952); D. L. Bunker and M. Pattengill, *ibid.* 48, 772 (1968); S. A. Safron, N. D. Weinstein, D. R. Herschbach, and J. C. Tully, Chem. Phys. Lett. 12, 564 (1972); W. L. Hase and R. J. Wolf, J. Chem. Phys. 71, 2911 (1979).

<sup>7</sup>D. M. Wardlaw and R. A. Marcus (in preparation).

<sup>8</sup>A. F. Turfa, D. E. Fitz, and R. A. Marcus, J. Chem. Phys. 67, 4463 (1977). <sup>9</sup>D. M. Wardlaw, Ph. D. thesis, University of Toronto, 1982.

<sup>10</sup>A. F. Wagner and E. K. Parks, J. Chem. Phys. 65, 4343 (1976).

In Ref. 1 the action variables were written as Nh, in units of h = 1, and the canonically conjugate angle variables covered a range (0, 1). In the present paper an equivalent choice is made in which the actions are Nh, in units of h = 1, and the canonically conjugate angles cover an interval  $(0, 2\pi)$ .

<sup>12</sup>C. Kittel, W. D. Knight, and M. A. Ruderman, Berkeley Physics Course (McGraw-Hill, New York, 1965), Vol. 1.

<sup>13</sup>F. James, Rep. Prog. Phys. 43, 1145 (1980).

<sup>14</sup>D. L. Bunker, J. Chem. Phys. 40, 1946 (1964); S. C. Farantos, J. N. Murrell, and J. J. Hadjuk, Chem. Phys. 68, 109 (1982).

<sup>15</sup>(a) J. D. Doll, Chem. Phys. Lett. **72**, 139 (1980); L. B. Bhuiyan and W. L. Hase, J. Chem. Phys. **78**, 5052 (1983); (b) J. Doll, *ibid*. **73**, 2760 (1980); **74**, 1074 (1981).

<sup>16</sup>D. W. Noid, M. L. Koszykowski, M. Tabor, and R. A. Marcus, J. Chem. Phys. 72, 6169 (1980); M. V. Berry, Ann. Phys. 131, 163 (1981).

<sup>17</sup>J. E. Adams, J. Chem. Phys. 78, 1275 (1983).

<sup>18</sup>R. Viswanathan, L. M. Raff, and D. L. Thompson, J. Chem. Phys. 81, 3118 (1984).

M. Quack and J. Troe, Ber. Bunsenges. Phys. Chem. 78, 240 (1974).
 W. L. Hase, J. Chem. Phys. 64, 2442 (1976).

<sup>21</sup>R. J. Duchovic, W. L. Hase, B. Schlegel, M. J. Frisch, and K. Raghavachari, Chem. Phys. Lett. 89, 120 (1982). These authors calculated an ab initio potential energy surface for the CH₄→CH₃ + H reaction. The results indicated a deficiency similar to that discussed in the text, when a Morse model was fitted to the ab initio C-H bond-fission potential.

<sup>22</sup>For example, a Morse potential with  $\beta$  increasing by a factor 1.5 at  $r-r_e=3$  Å is known to represent the  $H_2$  potential curve (Ref. 19), and an ab initio calculated stretching potential for  $CH_4 \rightarrow CH_3 + H$  can be fitted by a Morse function with  $\beta$  represented by a cubic polynomial in  $r-r_e$ . [R. J. Duchovic and W. L. Hase, Chem. Phys. Lett 110, 474 (1984)].

<sup>23</sup>This Varshni potential as a function of the ON-O distance x is  $D\{1-(x_e/x)\exp[-\beta(x^2-x_e^2)]\}$ . In the extensive comparative study of internuclear potential functions [D. Steele, E. R. Lippincott, and J. T. Vanderslice, Rev. Mod. Phys. **34**, 239 (1962)] the Varshni function was found to be one of three providing a superior description of the homo- and heteronuclear diatomics considered.

<sup>24</sup>R. J. Duchovic, W. L. Hase, and H. B. Schlegal, J. Phys. Chem. 88, 1339 (1984).

<sup>25</sup>M. Quack, J. Phys. Chem. 83, 150 (1979).

<sup>26</sup>(a) J. Troe, J. Chem. Phys. **79**, 6017 (1983); (b) J. Phys. Chem. **83**, 114 (1979).

<sup>27</sup>(a) W. Forst, *Theory of Unimolecular Reactions* (Academic, New York, 1973); (b) G. Z. Whitten and B. S. Rabinovitch, J. Chem. Phys. **38**, 2466 (1963).

<sup>28</sup>In classical trajectory calculations of the recombination rate constant for  $H + CH_3 \rightarrow CH_4$  at T = 300 K the calculated rate increased by an order of magnitude when a Morse function rather than *ab initio* curve (Ref. 22) was used for the C-H stretching, perhaps because of the relatively low value of  $E'_{\infty}$  at 300 K.

<sup>29</sup>H. Goldstein, *Classical Mechanics* (Addison-Wesley, Reading, MA, 1950),  $A^{-1}(\psi, \theta, \varphi)$  is given in Eq. (4-47) of p. 109.

<sup>30</sup>G. R. Bird, J. C. Baird, A. W. Jache, J. A. Hodgeson, R. F. Curl, A. C. Kunkle, J. W. Bransford, J. Rastrup-Anderson, and J. Rosenthal, J. Chem. Phys. 40, 3378 (1964).

<sup>31</sup>G. Herzberg, Electronic Spectra of Polyatomic Molecules (Van Nostrand, New York, 1967).

<sup>32</sup>JANAF Thermochemical Tables, 2nd ed., NSRDS Natl. Bur. Stand. No.

- 37 (U. S. GPO, Washington, D.C., 1971).
- <sup>33</sup>M. Quack and J. Troe, Ber. Bunsenges, Phys. Chem. 81, 329 (1977).
- <sup>34</sup>R. A. Bair and W. A. Goodard (private communication).
- 35T. Shimanouchi, J. Chem. Phys. Ref. Data 6, 1018 (1977).
- <sup>36</sup>P. Botschwina, W. Mayer, and A. M. Semkow, Chem. Phys. 15, 25 (1976).
- <sup>37</sup> Tables of Bond Dissociation Energies for Simple Molecules, NSRDS Natl.
- Bur. Stand. No. 31 (U. S. GPO, Washington, D.C., 1970).

  38T. H. Dunning and N. W. Winter, J. Chem. Phys. 63, 1847 (1975), and references cited therein.
- <sup>39</sup>P. A. Giguere, in Complements au Nouveau Traite de Chimie Minerale, edited by P. Pascal (Masson et Cie, Paris, 1975), Vol. 4.
- <sup>40</sup>G. Herzberg, Spectra of Diatomic Molecules (Van Nostrand, New York, 1950).
- <sup>41</sup>J. Troe, J. Phys. Chem. 88, 4375 (1984).
- <sup>42</sup>A. Warshel, in Semiempirical Methods of Electronic Structure Calculation, Part A: Techniques, edited by G. A. Segal (Plenum, New York, 1977).
- <sup>43</sup>W. A. Goddard (private communication).

- <sup>44</sup>I. Kakagawa and T. Shimanouchi, J. Mol. Spectrosc. 39, 255 (1971), (cf. set A in Table VII there.)
- <sup>45</sup>W. J. Chesnavitch and M. T. Bowers, J. Chem. Phys. 66, 2306 (1977).
- <sup>46</sup>The following identity is used:  $(\mathbf{a} \times \mathbf{b}) \times (\mathbf{c} \times \mathbf{d}) = [\mathbf{a} \cdot (\mathbf{b} \times \mathbf{d})]$   $\mathbf{c} [\mathbf{a} \cdot (\mathbf{b} \times \mathbf{c})] \mathbf{d}$  with  $\mathbf{a} = \mathbf{c} = \mathbf{l}$ ,  $\mathbf{b} = \mathbf{k}$ ,  $\mathbf{d} = \mathbf{j}_i$ . One thus finds  $\sin \beta_i = \cos \theta_{ix} / \sin \theta_{ii}$ , where  $\theta_{ix}$  is the angle between  $\mathbf{j}_i$  and  $\mathbf{l} \times \mathbf{k}$ . The above vector identity with  $\mathbf{a} = \mathbf{l}$ ,  $\mathbf{b} = \mathbf{d} = \mathbf{k}$ , and  $\mathbf{c} = \mathbf{j}_i$  yields  $\cos \theta_{ix} = \mp \sin \theta_{ki} \sin \alpha_k$ . Equation (E7) of the text follows from the last two results.
- <sup>47</sup>M. Tinkham, Group Theory and Quantum Mechanics (McGraw-Hill, New York, 1964), p. 246.
- <sup>48</sup>R. K. Pathria, Statistical Mechanics (Pergamon, Oxford, 1972), pp. 459–460
- <sup>49</sup>I. S. Gradshteyn and I. W. Ryzhik, *Table of Integrals, Series and Products* (Academic, New York, 1965), pp. 1039-1040.
- <sup>50</sup>E. V. Waage and B. S. Rabinovitch, Chem. Rev. 70, 377 (1970).